inorganics

MDPI

Review

Integration of CO_2 Capture and Conversion by Employing Metal Oxides as Dual Function Materials: Recent Development and Future Outlook

Wei Jie Tan and Poernomo Gunawan *

School of Chemistry, Chemical Engineering and Biotechnology, Nanyang Technological University, 62 Nanyang Drive, Singapore 637459, Singapore; c210023@e.ntu.edu.sg

* Correspondence: pgunawan@ntu.edu.sg

Abstract: To mitigate the effect of CO_2 on climate change, significant efforts have been made in the past few decades to capture CO_2, which can then be further sequestered or converted into value-added compounds, such as methanol and hydrocarbons, by using thermochemical or electrocatalytic processes. However, CO_2 capture and conversion have primarily been studied independently, resulting in individual processes that are highly energy-intensive and less economically viable due to high capital and operation costs. To enhance the overall process efficiency, integrating CO_2 capture and conversion into a single system offers an opportunity for a more streamlined process that can reduce energy and capital costs. This strategy can be achieved by employing dual function materials (DFMs), which possess the unique capability to simultaneously adsorb and convert CO_2. These materials combine basic metal oxides with active metal catalytic sites that enable both sorption and conversion functions. In this review paper, we focus on the recent strategies that utilize mixed metal oxides as DFMs. Their material design and characteristics, reaction mechanisms, as well as performance and limitations will be discussed. We will also address the challenges associated with this integrated system and attempt to provide insights for future research endeavors.

Keywords: CO_2 capture; CO_2 conversion; dual function material; materials design

Citation: Tan, W.J.; Gunawan, P. Integration of CO_2 Capture and Conversion by Employing Metal Oxides as Dual Function Materials: Recent Development and Future Outlook. *Inorganics* **2023**, *11*, 464. https://doi.org/10.3390/inorganics11120464

Academic Editors: Roberto Nisticò, Torben R. Jensen, Luciano Carlos, Hicham Idriss, Eleonora Aneggi and Francis Verpoort

Received: 27 September 2023
Revised: 10 November 2023
Accepted: 22 November 2023
Published: 30 November 2023

1. Introduction

With the concentration of carbon dioxide (CO_2) in the earth's atmosphere increasing at an unprecedented rate, climate change has become one of the most pressing challenges of our time due to its adverse impact on environmental and ecological welfare, as reported by the Intergovernmental Panel on Climate Change (IPCC) [1]. Addressing this issue requires a comprehensive approach that encompasses CO_2 emission reductions, effective CO_2 storage, and the sustainable utilization of CO_2 as chemical feedstock to close the carbon cycle. Respectively, CO_2 capture and CO_2 conversion have garnered considerable attention as potential solutions to mitigate its impact and, concurrently, create other value-added products. These approaches are not only necessary to slow down global warming, but also to offer economic opportunities across various industries [2,3]. Naims shows that the economic feasibility for carbon capture and utilization (CCU) is specific to the technology; that it depends on the process efficiency in using CO_2 as a cheaper alternative feedstock to more expensive raw materials produced from fossil fuel [4].

Being primarily emitted from combustion processes, the strategies for CO_2 capture are determined by several factors, such as its partial pressure, operating conditions, and flue gas compositions. In general, there are typically three types of capture categories, as illustrated in Figure 1, namely (1) pre-combustion, (2) oxyfuel combustion, and (3) post-combustion, depending on the installation location [5]. A general comparison of their advantages and disadvantages in terms of their energy requirement, costs, CO_2 recovery, and limitations is presented in Table 1. Pre-combustion capture removes CO_2 before

combustion is completed. It is typically integrated with a gasifier or reformer where syngas is produced. Through the intermediate removal of CO_2, H_2-rich gas is obtained, which can be further used for heat/power generation. Oxyfuel combustion employs either nearly-pure oxygen environments for combustion, or chemical looping combustion (CLC), in which solid oxides are used as oxygen carriers, resulting in a high concentration of CO_2 that allows for more efficient and inexpensive separation. However, the combustion itself would be relatively costly due to high oxygen purity demands. Lastly, post-combustion capture removes CO_2 from the flue gas. It is considered the most established technology [5], where it typically employs liquid amine absorption or solid adsorption. Due to the low CO_2 partial pressure in the flue gas (*ca.* 10–15%), large volumes of gas, as well as large amounts of energy and equipment size are required, making post-combustion capture processes relatively expensive. For comparison, the mean capture cost from high CO_2 purity sources via oxyfuel combustion ranges from USD 10 to USD 50 per ton of CO_2 mitigated, while that from post-combustion flue gas amine scrubbing ranges from USD 50 to USD 120 [3]. Following its capture, high-purity CO_2 can be recovered via temperature or pressure swing regeneration, after which it is compressed and transported for storage (e.g., geological injection, mineralization) or further utilized or converted.

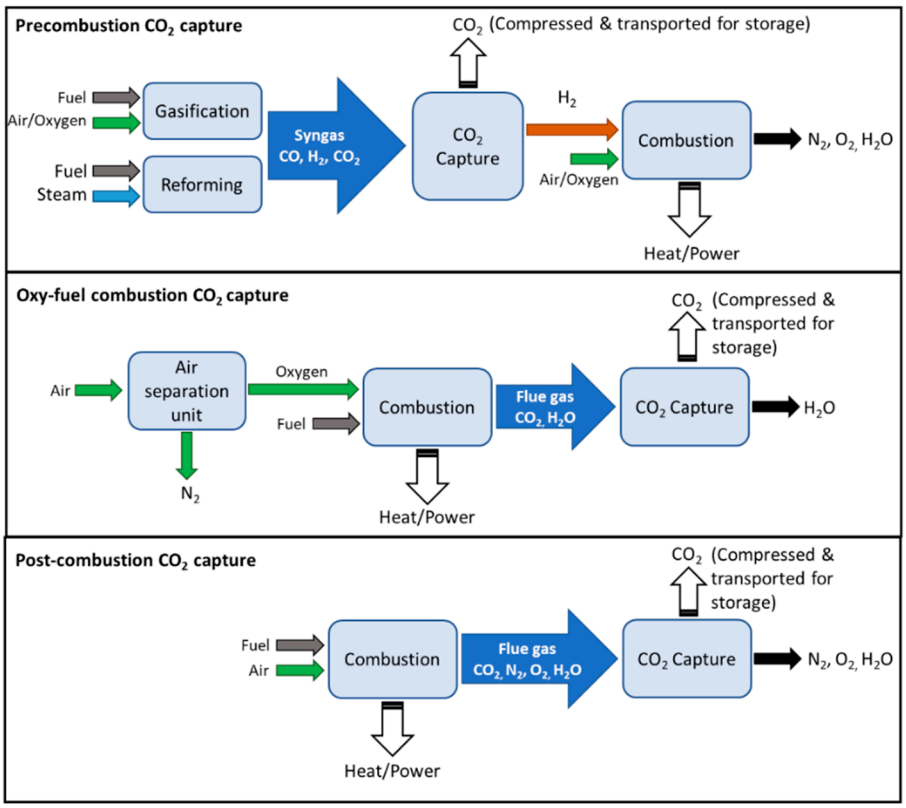

Figure 1. Schematic diagram of CO_2 capture processes from different sources of combustion.

Table 1. Comparison of different CO_2 capture categories. Reproduced from ref. [6] with permission from the American Chemical Society.

Category	Pre-Combustion	Oxyfuel Combustion	Post-Combustion	
			Amine Absorption	Solid Adsorption
CO_2 recovery	92–93%	90–94%	90–98%	80–95%
Energy requirement	low energy	low energy	high regeneration energy	high regeneration energy
Costs	less expensive	moderately expensive	expensive	expensive

Table 1. *Cont.*

Category	Pre-Combustion	Oxyfuel Combustion	Post-Combustion	
			Amine Absorption	Solid Adsorption
Challenges	increased process complexity high CO_2 concentration high pressure process	requires air separation unit high CO_2 concentration high temperature process	corrosion solvent degradation low CO_2 concentration	solid attrition high pressure drop easily poisoned by impurities (NO_x, SO_x) low CO_2 concentration

CO_2 conversion technologies seek to transform the captured CO_2 into useful chemicals, fuels, and materials. Although conversion processes may not directly lead to a net carbon reduction, it enables a circular utilization of CO_2 wastes as feedstock, which may reduce the overall carbon footprint of the corresponding chemical and fuel production, thus leading to more environmentally friendly production processes, as shown in a case study of polyol production for polyurethane [7]. A comprehensive review of sustainable CO_2 conversion by incorporating a life cycle assessment (LCA) in various CO_2 conversion pathways has been published by Artz et al. [8], who concluded that replacing energy-intensive feedstock with CO_2 seems highly promising, particularly when being integrated with renewable energy. In addition, as a C1 building block, the use of CO_2 may also create new, greener synthetic pathways [9].

Despite significant progress having been made for CO_2 capture and CO_2 conversion individually, numerous challenges remain for each technology, most notably the cost effectiveness and the process scalability. Generating high purity of CO_2 intermediates for subsequent utilization requires a large amount of energy for CO_2 recovery, the regeneration of the capture media, and the subsequent gas compression. The purified CO_2 stream then needs to be transported to the location where it will be converted to the desired product, thus further increasing energy demands. To address these issues, combining CO_2 capture and utilization in an integrated system, where in situ conversion will also serve to regenerate the capture media in the same reactor, would be a potential solution to eliminate both compression and transportation costs, thus making the whole process more economical and efficient. For example, the total energy required to produce 1 metric ton of methanol from separate direct air capture and hydrogenation reactions is about 49.4 GJ, out of which 27 GJ is consumed in the CO_2 capture, recovery, and distribution steps. For comparison, to achieve the same product yield, the integrated CO_2 capture and conversion (ICCC) system only requires less than 50% of the total energy requirement, as reported by Freyman et al. [10]. Additionally, ICCC could also reduce capital costs by approximately 38%, as fewer unit operations are required. Freyman et al. coined a term "Reactive Capture" to describe this ICCC system, the concept of which is depicted in Figure 2. To make this system work effectively, the optimization of the reaction conditions, the tuning of the material properties, as well as designing an appropriate reactor system configuration are necessary to ensure a good ICCC performance with good product selectivity and catalyst stability.

In this review paper, we will focus on the development of mixed metal oxides (MMO) as dual function materials (DFMs). To perform both CO_2 capture and CO_2 conversion, DFMs typically are synthesized as a combination of a CO_2 sorbent and a catalytic component. In the presence of CO_2 and other secondary reactants (e.g., H_2, for the methanation of CO_2), the sorbent component first captures CO_2, which then reacts with secondary reactants on the active catalytic sites, converting it into final products [10]. A schematic diagram of ICCC with DFMs is illustrated in Figure 3. The efficiency of the DFM would therefore depend on the CO_2 capture capacity and selectivity, as well as its catalytic activity. Among various solid sorbents, the choice of metal oxides, particularly alkali and alkaline earth oxides, as the sorbent component of a DFM, is convenient, in that the catalytic component would typically also be a transition or noble metal, which can be facilely

incorporated into the DFM during its synthesis, such as via co-precipitation or incipient wetness impregnation.

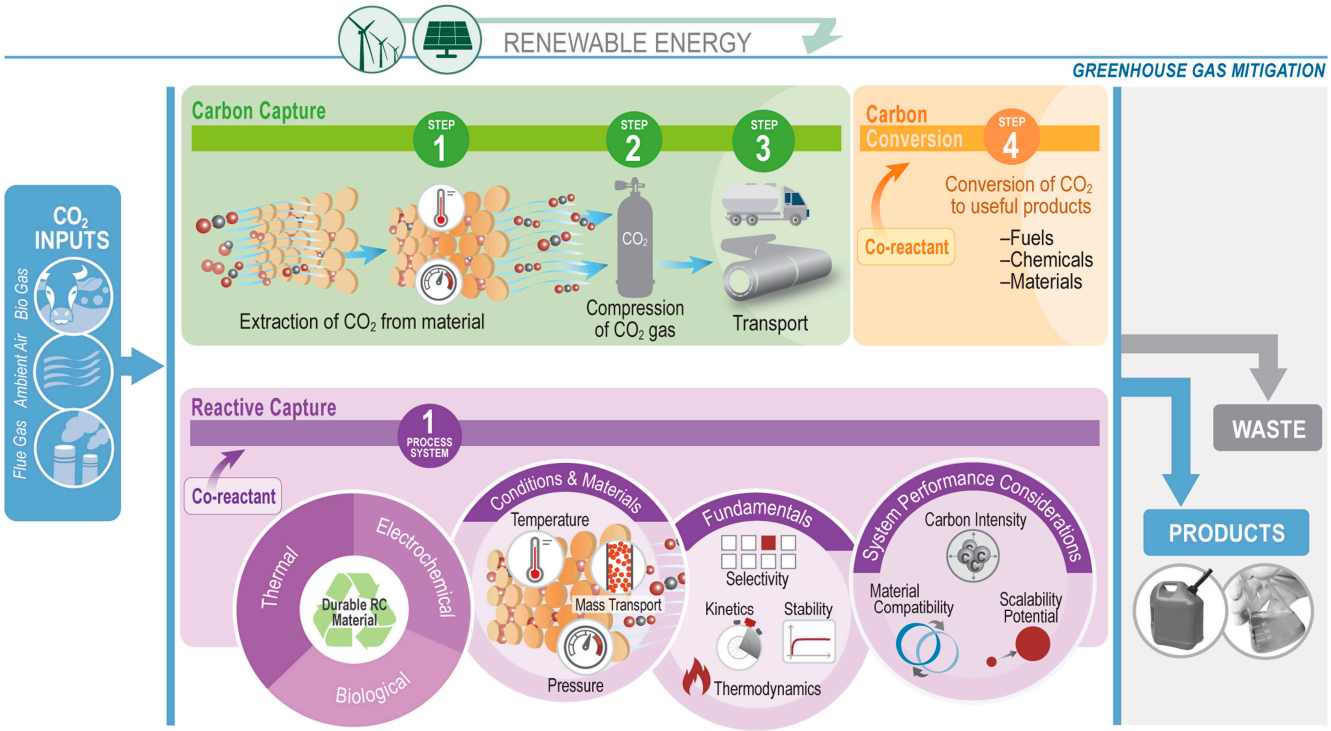

Figure 2. Integrated CO_2 capture and conversion system (Reactive Capture, bottom) in comparison with separate processes. Reprinted from ref. [10] with permission from Elsevier.

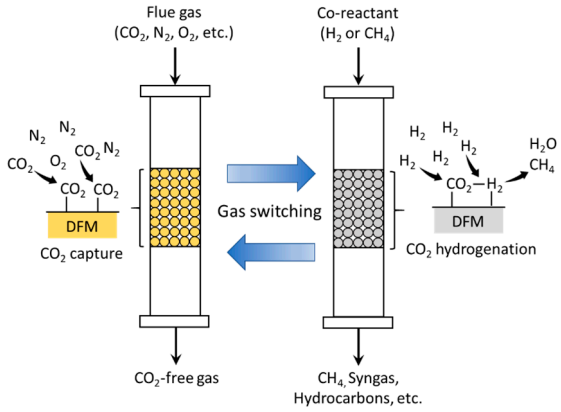

Figure 3. Schematic diagram of integrated CO_2 capture and conversion using DFMs.

To give an overview of the recent trends in this field, we have carried out a literature search on the Web of Science database with the following keywords:

"dual function material" AND "CO_2 capture" AND "CO_2 conversion"
"dual function material" AND "CO_2 capture" AND "CO_2 utilization"

It was found that about 60 relevant papers were published in the span of 10 years, between 2012 and 2022. Farrauto et al. were among the pioneering research groups who first published their work on the development of a DFM in 2015, which comprised ruthenium as the methanation catalyst and nano-dispersed CaO as the CO_2 sorbent, which are both supported on a porous γ-Al_2O_3 carrier [11]. The synthesized material was able to adsorb CO_2 and convert it in the same reactor into synthetic natural gas by using H_2 gas as the co-reactant at 320 °C. Upon the introduction of steam into the reactor, the material

showed a stable methanation performance with more than 99% CH_4 purity after 20 cycles. The initial success of this experiment has since gathered increasing interests to explore DFM systems, as indicated by the increasing number of publications in recent years (Figure 4). We have seen efforts being made to improve the CO_2 capture capacity, conversion, and selectivity while reducing the precious metal content. The first review paper on DFMs was published in 2019 by Melo Bravo and Debecker [12], which focused on combined CO_2 capture and methanation, followed by several others in 2020 [6] and 2021 [13–16]. The highlights of these review papers are summarized in Table 2.

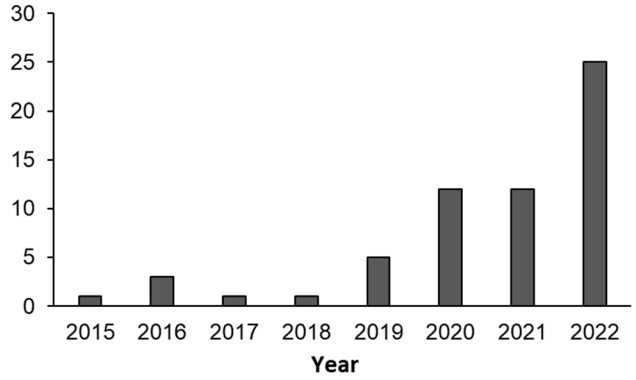

Figure 4. Annual number of publications in the field of dual function materials for integrated CO_2 capture and conversion (2015–2022).

Table 2. Summary of the published reviews on dual function materials (DFMs) for integrated CO_2 capture and conversion.

Authors	Year	Brief Description	Reference
Melo Bravo and Debecker	2019	Early review of DFMs with focus on CO_2 methanation reaction and different types of reactor configurations	[12]
Omodolor et al.	2020	Overview of oxide- and carbonate-based CO_2 adsorbents	[6]
		Investigation of the active metals, material characteristics, and reaction conditions for Ni-, Ru-, and Rh-based DFMs in CO_2 methanation, DRM, and RWGS reactions	
		Brief discussion on hydrotalcite-supported Fe-Cr-Cu catalyst as well as promoted Cu supported on alumina for syngas production	
Merkouri et al.	2021	Chronological review of advances in DRM, RWGS, and CO_2 methanation, as well as evaluation of the reaction mechanism of DFMs, by relating their performances with their physicochemical properties	[13]
Sun et al.	2021	Investigation of the process parameters and adsorbent–catalyst interaction on high-temperature CO_2 capture combined with in situ DRM, RWGS, and methanation reactions	[14]
Sabri et al.	2021	Environmental and economic evaluation of CO_2 capture and utilization process integration, as well as catalyst development for CO_2 conversion in various systems, such as photocatalysis, electrocatalysis, and thermocatalysis	[15]
Li et al.	2021	Discussion on the performances of dual-function oxide particles for CO_2 capture integrated with DRM, CO_2 hydrogenation, and chemical looping	[16]

DRM: dry reforming of methane; RWGS: reverse water–gas shift.

To continue building upon the previous reviews, herein we aim to cover the latest developments on the application of DFMs that employ solid metal oxides for ICCC, particularly from 2021–2023. We will begin our discussion by first giving an overview of the principles of CO_2 capture with metal oxides as solid sorbents, as well as the catalytic

conversion of CO_2 from thermodynamic and material perspectives, followed by the typical synthetic methods of DFMs. Thereafter, the performance of various DFMs in ICCC systems will be further assessed for key reactions, such as methanation, RWGS, and DRM, by evaluating key metrics such as the CO_2 capture capacity, selectivity, reaction conversion, and stability. We will correlate these metrics with material design parameters, such as the types of metal oxides used as adsorbents, metallic active sites as catalysts, and the synthetic methods. Mechanistic studies on the molecular interaction between CO_2 and the adsorption and catalytic active sites will also be presented to shed some light on the relationship between the materials' physicochemical properties and their performance. As a conclusion, we will present our perspectives, as well as an outlook on the future opportunities with the emerging technologies of ICCC with DFMs.

2. Metal Oxides as Sorbents for CO_2 Capture

Various CO_2 capture methods have been extensively studied and explored, and several excellent reviews have been recently published [17–28]. An overview of these technologies is presented in Figure 5, among which, liquid absorption in organic amines, such as methanolamine (MEA) and n-methyldiethanolamine (MDEA), have seen the most implementation in large demonstration plants worldwide [29] due to its high absorption capacity. However, this system requires a high energy consumption for amine regeneration, which is prone to degradation. It is also highly corrosive, thus leading to high operating and capital costs.

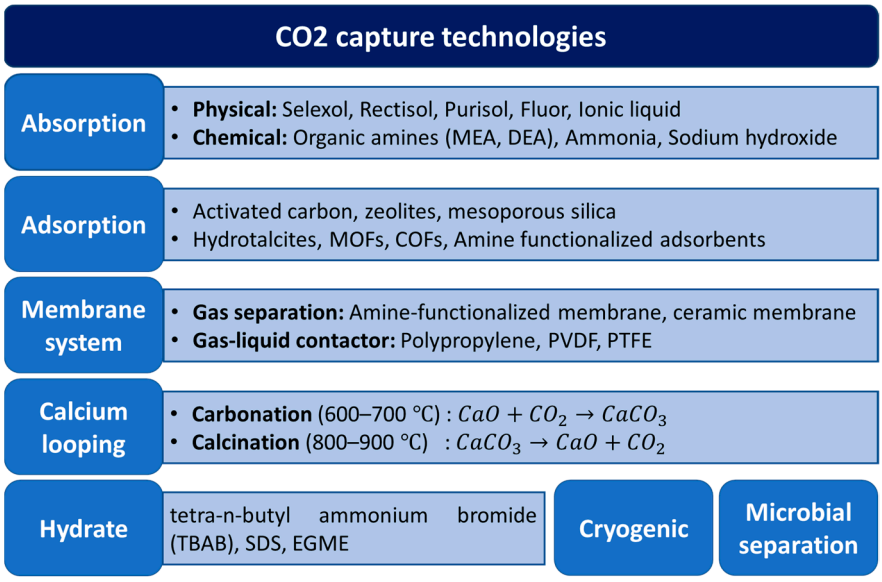

Figure 5. Overview of CO_2 capture technologies.

As potential alternatives to liquid absorption, solid sorbents, such as zeolites [30], hydrotalcites [17,20,31,32], magnesium oxides [33–36], metal organic frameworks (MOFs) [23,37], and porous organic polymers (POPs) [38–40], have been studied extensively due to their easy regeneration and tunable pore size and surface properties. Given their wide variety, the suitability of solid adsorbents depends on their application temperatures, typically ranging from low temperatures (<200 °C) for MOFs, POPs, and zeolites to medium temperatures (200–400 °C) for hydrotalcites and MgO-based sorbents. An overview of commonly used solid sorbents and their typical application temperatures is presented in Figure 6.

In principle, their CO_2 capture capability primarily relies on the physical adsorption of CO_2 without forming a chemical bond. Physisorption is typically mildly exothermic (−25 to −40 kJ/mol) and requires less energy for regeneration as compared to chemisorption processes. Owing to its exothermic nature, the adsorption of CO_2 decreases at a higher temperature, making it more suitable for low-to-medium operating temperatures (<400 °C). However, physisorption processes are usually less selective, leading to the adsorption of

other gases, such as N_2 and water vapor, thus lowering the adsorption capacity of CO_2, which is the primary challenge that needs to be solved in order to scale up their application. A common strategy to improve the CO_2 adsorption capacity is by increasing the basicity of the materials via the incorporation of alkaline metals, such as K and Na, though their amounts should be carefully studied as high metal loading may decrease the surface area of the material. For example, for hydrotalcite-based materials, many attempts have been made to modify Mg/Al-based hydrotalcites with K [41–45], Na [43,46], and Cs [42,43,47], with typical optimum K loading of about 20 wt% to achieve the maximum sorption capacity at temperatures between 300 and 400 °C.

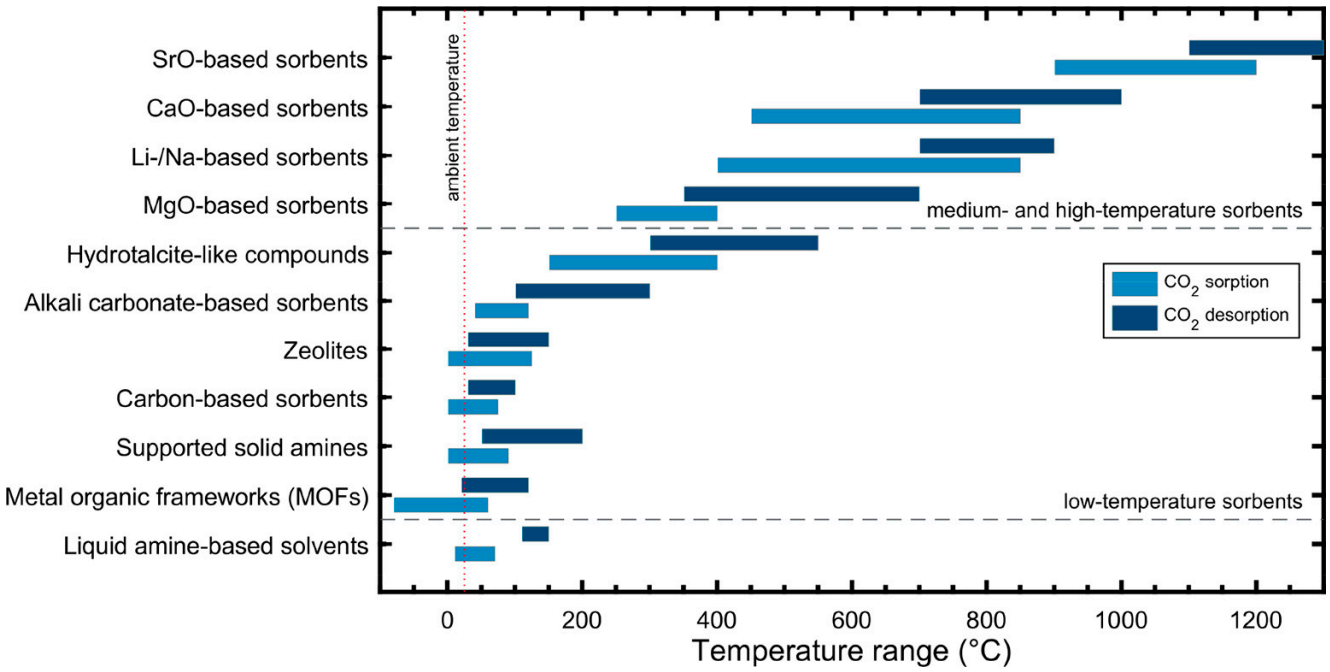

Figure 6. Overview of commonly used solid sorbents and their typical application temperatures. Liquid amine system is shown as the basis for comparison. Reprinted from ref. [25] with permission from the American Chemical Society.

On the other hand, for high-temperature CO_2 adsorption (see Figure 6), calcium looping has been found to be a promising technology [25,48]. It utilizes CaO to react with CO_2 to form calcium carbonate (carbonation), which can be calcined back to CaO for reuse, while recovering high-purity CO_2, as shown in Equation (1).

$$CaO_{(s)} + CO_{2(g)} \leftrightarrow CaCO_{3(s)} \Delta H^{o}_{298K} = -178 \frac{kJ}{mol} \quad (1)$$

Owing to its low cost and high theoretical sorption capacity of up to 78.6 wt% (17.8 mmol CO_2/g sorbent), CaO has been extensively studied, and a pilot scale of this technology has been implemented in cement production [49,50]. An economic feasibility study by MacKenzie et al. shows that calcium looping is highly competitive with liquid amine-based systems [51]. However, to fully realize the industrial applications of the CaO sorbent, its material stability upon prolonged use at a high temperature needs to be improved as it is susceptible to sintering and surface carbonate poisoning [52], which may significantly decrease its CO_2 sorption capacity and limit its recyclability over time.

Extensive amounts of work have been devoted to the study and development of CaO-based sorbents for CO_2 capture, the kinetic and thermodynamic perspectives on the mechanisms of CO_2 sorption, as well as methods to improve the performance of the sorbents by mitigating their drawbacks [52–55]. The forward, highly exothermic carbonation of CaO with CO_2 and the backward, endothermic calcination of $CaCO_3$ as described in

Equation (1) occur at temperature ranges of 600–900 °C [53,55]. The calcination reaction typically takes place at a higher temperature than the carbonation reaction. However, at such temperature ranges, CaO-based CO_2 adsorbents may suffer from sintering, a phenomenon of the agglomeration of adsorbent particles when operating temperatures exceed the Tammann temperature (T_T), at which the mobility of the grains/crystallites in the solid material becomes appreciable, leading to major changes in the particle morphology. Given that T_T of $CaCO_3$ is typically about 533 °C [56], CaO crystallite growth would primarily occur during the calcination step of $CaCO_3$. As a result, particle sintering is inevitable under repeated carbonation–calcination cycles [57].

Lysikov et al. studied the behavior of CO_2 uptake by different CaO precursors in a series of carbonation–calcination cycles in the temperature range of 750–850 °C, where they observed that post-calcination CaO does not fully re-carbonate, and that the amount of unreacted CaO increases from cycle to cycle until it forms a rigid interconnected CaO skeleton after multiple cycles, as shown in Figure 7 [58]. They, therefore, proposed a model in which, upon repeated cycles, small unreacted CaO grains agglomerate, grow into larger, denser clusters, and ultimately form a stable, non-porous recalcitrant CaO skeleton that is resistant to further sintering, as illustrated in Figure 8.

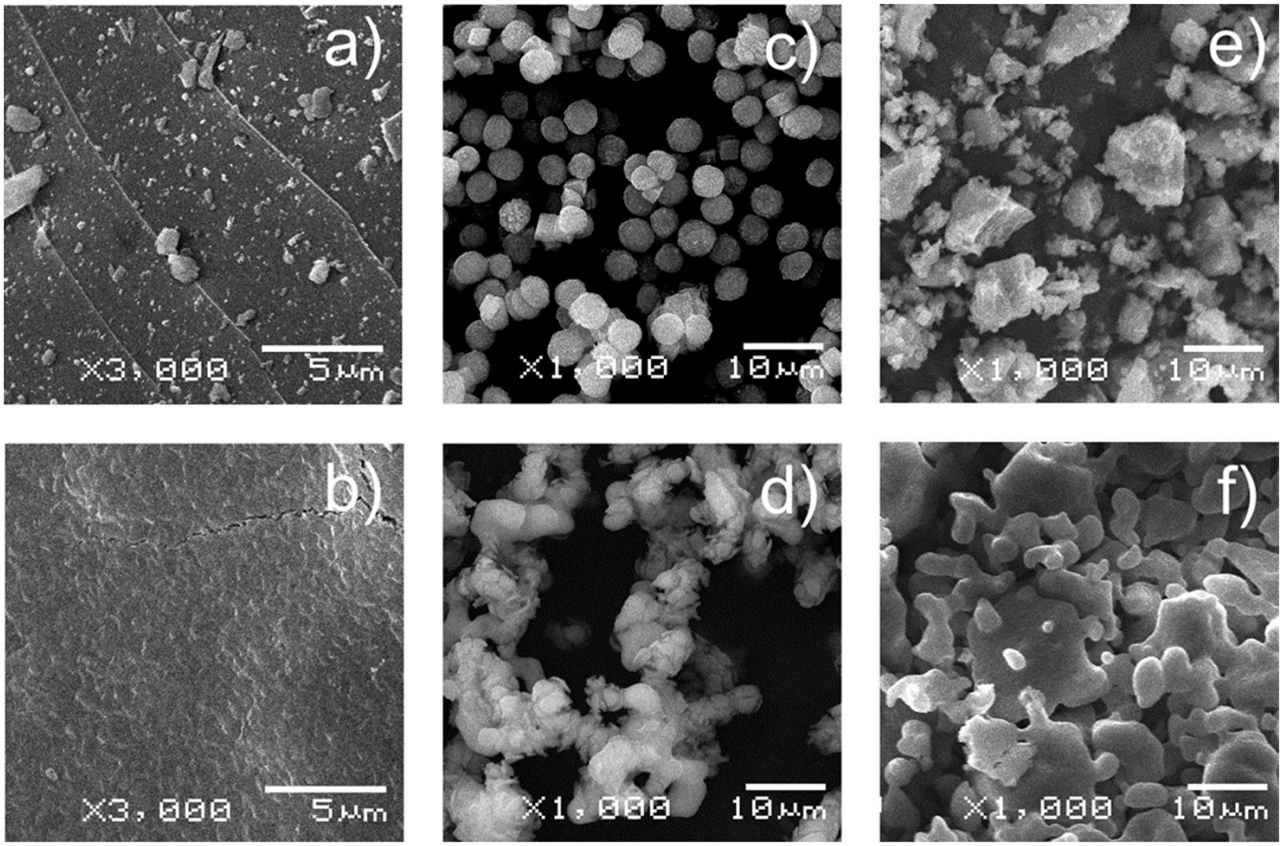

Figure 7. SEM images of the fresh CaO precursors: (**a**) MC, (**c**) MD, and (**e**) CP; and of the sorbents after carbonation–calcination cycles: (**b**) MC (211 cycles), (**d**) MD (86 cycles), and (**f**) CP (136 cycles). MC: monocrystal-derived sample, MD: monodispersed particles, CP: commercial powder. Reprinted from ref. [58] with permission from the American Chemical Society.

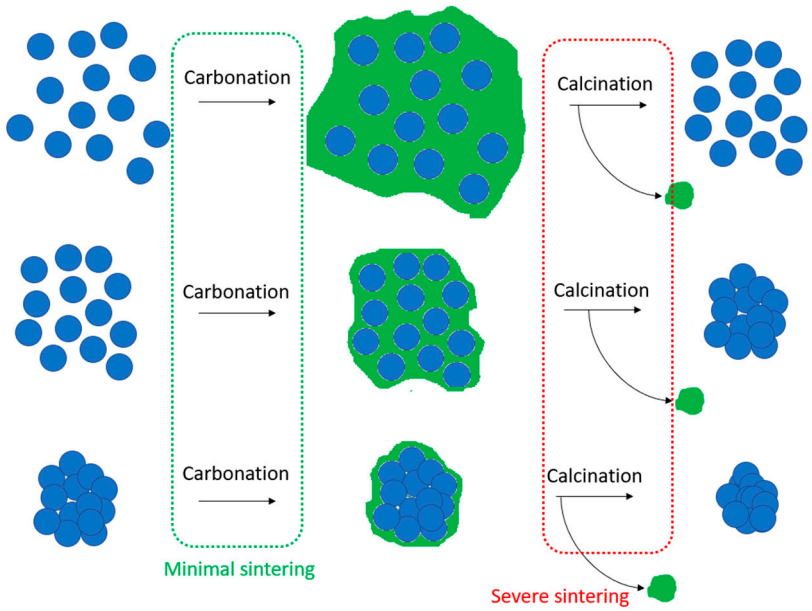

Figure 8. An illustration of the sintering process—blue spheres represent CaO-based adsorbent particles, and the green layer represents the formation of $CaCO_3$. Adapted from Lysikov et al. [58].

The sintering phenomenon shows to be destructive to the internal structure of the CaO-based sorbent, as it significantly reduces the particle surface area and pore volume due to the large, non-porous aggregate formation, which will eventually adversely affect the CO_2 sorption capacity with each carbonation–calcination cycle [59].

The common method of investigating the CO_2 sorption capacity of an adsorbent is thermogravimetric analysis (TGA), as depicted in Figure 9, which records the adsorbent's mass increase during carbonation and mass decrease during calcination. It can be seen that CO_2 uptake drastically decreases in the first few cycles, as reflected by the rapid decline of the sample weight after repeated carbonation–calcination reactions. CaO conversion to $CaCO_3$ decreased from an initial conversion of about 60% to a residual conversion of about 7–8%. This observation is in agreement with the model proposed by Lysikov et al. where the unreacted fraction of CaO increases with every cycle and only the outer layer of the non-porous recalcitrant CaO skeleton is carbonated, leading to a relatively constant residual conversion after sufficient cycles.

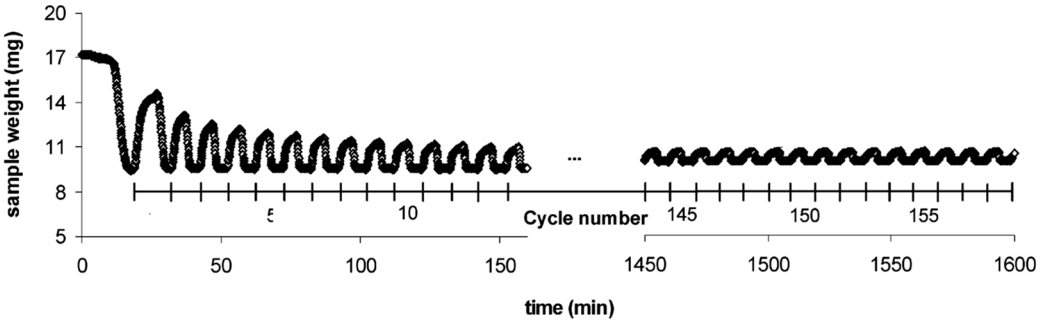

Figure 9. The profile of weight change vs. time for repeated calcination/carbonation cycles of limestone ($CaCO_3$). Calcination temperature is 850 °C; carbonation temperature is 650 °C. Reprinted from ref. [59] with permission from the American Chemical Society.

Meanwhile, kinetic analysis reveals that CO_2 adsorption characteristically takes place in two stages [52,54,55]—a fast, reaction-controlled stage, reflected by a spike in Figure 10 (first stage), followed by a slow, diffusion-controlled stage, reflected by a plateau in Figure 10 (second stage). As illustrated in Figure 11, in the reaction-controlled stage,

carbonation may occur wherever CO_2 molecules come into contact with the exposed CaO. The rate of carbonation is then dependent on the rate at which CO_2 molecules reach the CaO surface, which in turn might be affected by internal characteristics such as pore structures and porosity. As the carbonation proceeds, a layer of $CaCO_3$ forms on the unreacted CaO particle. Following this, the reaction then transitions into the diffusion-controlled stage where incoming CO_2 molecules must diffuse through the $CaCO_3$ layer to be in contact with any unreacted CaO. Consequently, the rate of carbonation decreases drastically as it now becomes limited by mass transfer.

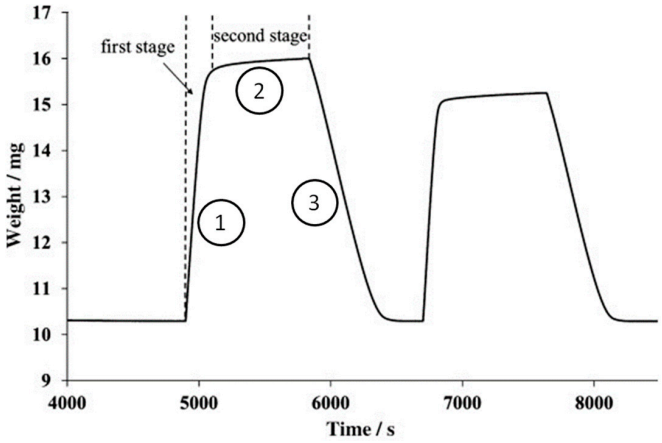

Figure 10. Typical carbonation–calcination cycle of CaO: (1) Fast carbonation stage, (2) Slow carbonation stage, and (3) Calcination step, as observed through thermogravimetric analysis (TGA). Reprinted from ref. [60] with permission from Wiley-VCH.

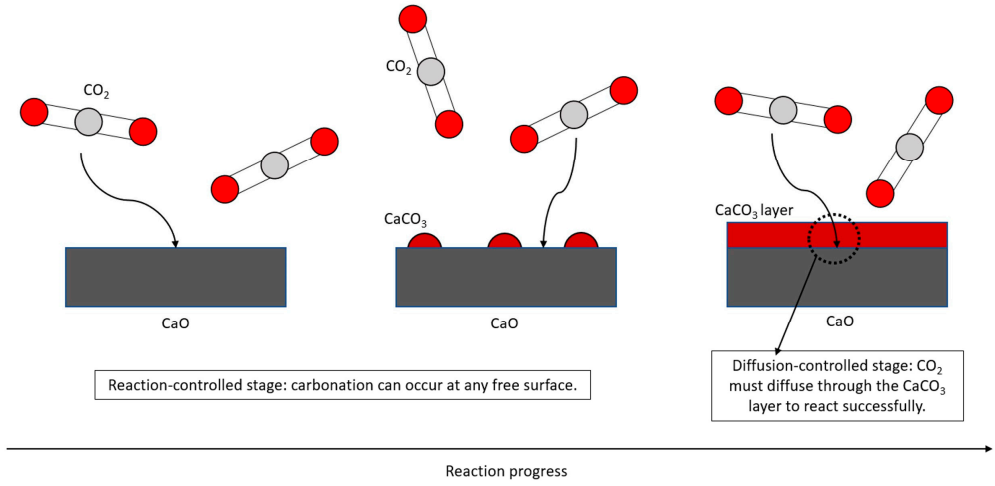

Figure 11. Illustration of the carbonation reaction mechanism of CaO. Adapted from Sun et al. [55] with permission from Elsevier.

The observed phenomena above allow us to glean important governing principles in the design of novel CO_2 sorbents, which can be incorporated into the synthesis of DFMs. Firstly, an ideal sorbent should be resistant to sintering at the required sorption temperatures to ensure its stability and prolonged use. In the case of CaO, metal supports such as the oxides of Al [61–64], Mg [65–67], and Yb [68,69], among many others, are commonly employed. These supports enhance an adsorbent's performance in numerous ways. For instance, certain metal oxides with high T_T can be used to decorate CaO particles [67], as in the case of MgO (T_T = 1276 °C), which helps enhance the stability of the material. Others form stable oxides that disperse CaO particles and thus physically retard the sintering process, as in the case of Yb_2O_3 [68]. Some other metals aid in dispersion by forming

composite metal oxides with CaO, as in the case of $Ca_{12}Al_{14}O_{33}$ and $Ca_3Al_2O_6$ [64]. These improvements allow supported sorbents to withstand severe reaction conditions while retaining CO_2 sorption capacities.

Secondly, an ideal sorbent should have a high internal surface area to allow for large sorption sites. The specific surface area measured via the Brunauer–Emmett–Teller (BET) method and the pore size measured with the Barrett–Joyner–Halenda (BJH) model are two common characteristics used to provide some insight into the internal morphology and microstructure of a sorbent. Primarily, the choice of synthetic method strongly influences the internal structures, and consequently, the specific surface area, of a sorbent [64]. Several studies evaluate the effect of various preparation methods on the sorbent's performance and show that sol–gel methods and flame spray pyrolysis, for example, produce sorbents with higher surface areas compared to those synthesized via simpler methods, such as the co-precipitation or mixing of metal precursor solutions (e.g., metal nitrate solutions). The choice of precursor chemicals seems also to influence the surface areas of a sorbent. It is expected that different chemical species will have varying interactions with CaO, giving rise to a variety of internal structures by the end of the synthesis depending on the chemical species present [55,70–72].

3. Overview of CO_2 Catalytic Conversion

Owing to its molecular structure, CO_2 is thermodynamically stable, as reflected in Figure 12, which compares the Gibbs free energy of formation (ΔG_f^o) for different carbon-containing compounds. Having the highest carbon oxidation state and lowest Gibbs free energy state, the chemical transformation of CO_2 will require considerable amounts of energy and, therefore, can only be achieved under harsh reaction conditions, such as a high temperature and pressure, leading to large energy penalties.

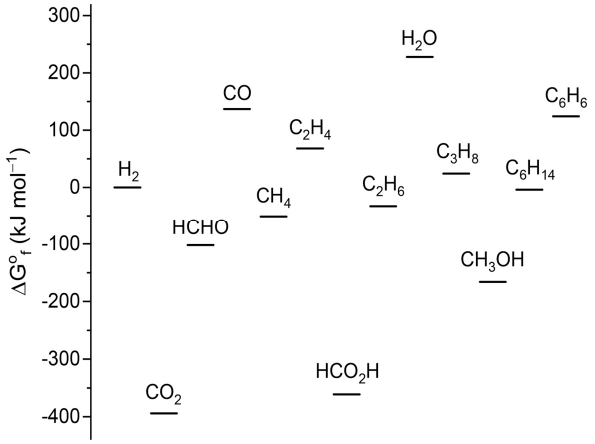

Figure 12. Gibbs free energy of formation (ΔG_f^o) for different carbon-containing compounds, including that of H_2 and H_2O as common co-reactants. Reprinted from Ref. [73] with permission from the American Chemical Society.

A strategy to make CO_2 transformation more thermodynamically favorable is by reacting it with a co-reactant that has a higher Gibbs free energy. For instance, the direct production of CO from CO_2 as a single reactant requires a large positive Gibbs free energy change (Equation (2)), whereas reacting it with H_2 significantly reduces the Gibbs free energy change of the reaction (Equation (3)). Consequently, most CO_2 transformations have been carried out by using a co-reactant, usually H_2, to produce a wide range of products, from small oxygenates to long-chain hydrocarbons.

$$CO_{2(g)} \rightleftarrows CO_{(g)} + \frac{1}{2}O_{2(g)} \Delta G^o_{298K} = 257.2 \frac{kJ}{mol} \quad (2)$$

$$CO_{2(g)} + H_{2(g)} \rightleftarrows CO_{(g)} + H_2O_{(g)} \Delta G^o_{298K} = 28.6 \frac{kJ}{mol} \quad (3)$$

Another approach for a feasible process is through the addition of a solvent. For example, the gaseous phase conversion of CO_2 to formic acid is thermodynamically unfavorable (Equation (3a)), while conducting it in an aqueous phase in the presence of water makes the reaction slightly exergonic (Equation (3b)) [73].

$$CO_{2(g)} + H_{2(g)} \rightleftarrows HCOOH_{(g)} \Delta G^o_{298K} = 32.9 \frac{kJ}{mol} \quad (3a)$$

$$CO_{2(aq)} + H_{2(aq)} \rightleftarrows HCOOH_{(aq)} \Delta G^o_{298K} = -4 \frac{kJ}{mol} \quad (3b)$$

Given its inertness, extensive research efforts have been focused on tackling the high reaction energy barrier by designing more effective catalysts that convert CO_2 with good activity, selectivity, and stability. These metrics are important in designing the catalytic component of a DFM, which is usually in the form of supported noble metal or metal oxide nanoparticles that serve as the active sites for CO_2 activation. The typical reactions include the methanation of CO_2 (also known as the Sabatier reaction; Equation (4)) [74–76], a reverse water–gas shift reaction (RWGS, Equation (5)) [77–79], and the dry reforming of methane (DRM, Equation (6)) [80–82]. The resulting CO produced in the RWGS and DRM reactions can be further hydrogenated to produce methanol (Equation (7)) or further converted into long-chain paraffinic and olefinic hydrocarbons via Fischer–Tropsch synthesis (FTS, Equation (8a–c)) [83–85].

$$CO_2 \text{ methanation}: \ CO_2 + 4H_2 \rightarrow CH_4 + 2H_2O; \Delta H^o_R = -165 \frac{kJ}{mol} \quad (4)$$

$$\text{Reverse water} - \text{gas shift (RWGS)}: \ CO_2 + H_2 \rightarrow CO + H_2O; \Delta H^o_R = 41.2 \frac{kJ}{mol} \quad (5)$$

$$\text{Dry reforming of methane (DRM)}: \ CO_2 + CH_4 \rightarrow 2CO + 2H_2; \Delta H^o_R = 247.3 \frac{kJ}{mol} \quad (6)$$

$$\text{Methanol formation}: \ CO + 2H_2 \rightarrow CH_3OH; \Delta H^o_R = -90.6 \frac{kJ}{mol} \quad (7)$$

Fischer–Tropsch synthesis (FTS):

$$CO + (2n+1)H_2 \rightarrow C_nH_{2n+2} + nH_2O \quad (8a)$$

$$nCO + 2nH_2 \rightarrow C_nH_{2n} + nH_2O \quad (8b)$$

$$nCO + 2nH_2 \rightarrow C_nH_{2n+2}O + (n-1)H_2O \quad (8c)$$

Different types of transition metals are found to catalyze these reactions. For instance, Ni is commonly used for methanation and DRM reactions, Cu for the RWGS and subsequent hydrogenation to methanol, and Fe or Co for FTS. Owing to their low costs and high abundance, they are usually favored over their noble metal counterparts. However, many of these catalysts are prone to severe deactivation due to carbon deposition and sintering. Additionally, product selectivity would be an issue as the above reactions may all occur in parallel, which brings its complications, especially in industrial settings, where a certain reaction may be preferred to another. For example, the production of methanol via the RWGS pathway might be compromised by methanation occurring as an unwanted side

reaction. Therefore, noble metals such as Ru, Rh, Pd, and Pt, though being more expensive, have received considerable attention because of their resistance to deactivation as well as high selectivity toward the desired products, which allow for more efficient downstream processes [86–89].

Despite major progress having been made in the development of various catalysts, significant challenges still exist in optimizing robust and economical catalysts with a good catalytic performance that can be utilized on an industrial scale. Through the better understanding of the reaction mechanisms, we can identify key descriptors that influence the performance of the catalysts [90], which eventually determine the effectiveness of DFMs in capturing CO_2 and catalyzing reactions.

4. Dual Function Materials: Synthetic Methods

A typical investigation into the sorption and catalytic performances of a metal oxide-based DFM starts with the choice of the desired precursors. This depends largely on the independent variables and the goals of the research, where some works aim to compare the efficacies of various adsorbent components [91–93], some seek to elucidate the mechanisms underlying CO_2 sorption and conversion [94,95], and others seek to evaluate the real-world applicability of DFMs by subjecting them to experiments that mimic realistic conditions.

The choice of adsorbent, catalytic components, and the support are known to influence the quality and performance of the as-synthesized DFM. For example, in an investigation by Bermejo-López et al. [96], supported CaO and Na_2CO_3 on Al_2O_3 were used as the adsorbent components of DFMs, with Ru as the catalytic metal. Various such DFMs were synthesized with varying CaO or Na_2CO_3 loadings. In general, higher adsorbent loadings promote CO_2 adsorption and hydrogenation. However, since CaO exhibits stronger basicity than Na_2CO_3, the former exhibits higher CO_2 capture, as shown in Figure 13. Consequently, the former requires higher calcination and hydrogenation temperatures, as compared to the latter.

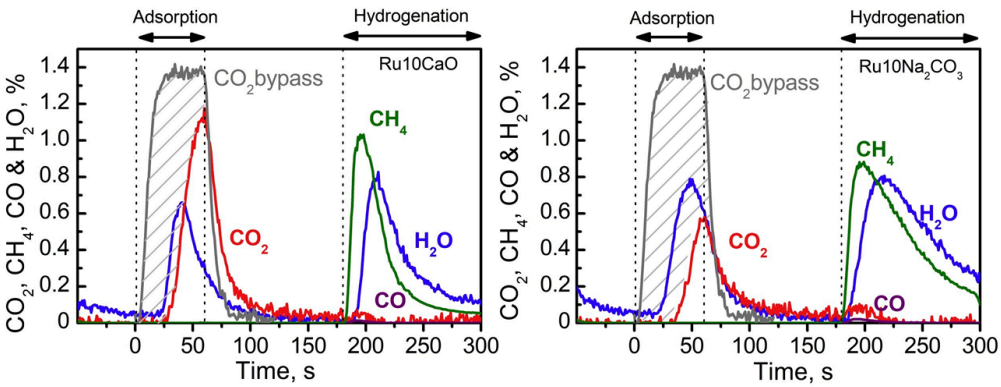

Figure 13. Concentration distribution profiles during a CO_2 adsorption and hydrogenation cycle at 370 °C with Ru10CaO and Ru10Na_2CO_3. Reprinted from ref. [96] with permission from Elsevier.

Upon deciding on the suitable precursors, the next step would be to employ an appropriate method to synthesize the DFM. Several synthetic methods are already well-known, which produce DFMs with certain desired characteristics, such as a high surface area and porosity, homogeneous particle dispersion, and unique morphology, with each of them having their respective benefits and disadvantages. A host of other factors also needs to be considered in selecting a synthetic method, including time, material, and labor costs, as well as ease of implementation, in addition to the typical structural characteristics. In this section, we will explore four commonly used methods, presented in an approximate order of their prevalence in the literature.

4.1. Incipient Wetness Impregnation

Incipient wetness impregnation (IWI) is a well-known and highly popular synthetic method for producing heterogeneous catalysts, and is, unsurprisingly, the method that is employed in most of the works on DFMs [11,91–101]. IWI is favored for its ease of implementation and relatively low costs [102]. This procedure aims to impregnate adsorbent and/or catalyst species onto a support by adding small amounts of adsorbent/catalyst precursor solution to a powdered support. The wet powder is then dried and may further be subjected to thermal activation treatment, e.g., calcination or reduction. The process is then repeated until the total volume of precursor solutions added equals the total pore volume of the support [103]. The final product is ideally a porous material with adsorbent and catalyst particles distributed throughout the surface area of the pores. Sietsma et al. found that the pore size distribution and drying rate affect the redistribution of the particles on the support, which eventually determines the final crystal size [102]. For supports with large pore size distribution, a fast drying rate leads to a larger crystal size due to a higher degree of particle redistribution. On the contrary, for supports with narrow pore size distribution, the effect of the drying rate is minimal.

Since surface area is one of the determinants in designing an effective DFM, the careful selection of the support materials, preferably ones with a larger surface area and well-defined pore structures, is an important consideration in optimizing the properties of DFMs after IWI post-treatment. Additionally, optimum loadings of adsorbent/catalyst components should be considered as well.

4.2. Sol–Gel Method

In order to gain greater control over the particles' morphology and porosity, sol–gel synthesis is an alternative method that can reliably ensure the formation of microstructures favorable to CO_2 capture, as well as uniform particulate dispersion and the minimal granulation of adsorbent/catalyst particles, owing to its ability to produce a solid-state material from a chemically homogeneous liquid precursor [104]. Sol–gel chemistry conventionally involves the hydrolysis and condensation of metal alkoxides, with reaction rates depending on the carbon length of the alkoxides (e.g., methoxide, ethoxide, propoxide, etc.) and the solvent/alkoxide ratio. A major limitation of the alkoxide-based synthetic method is the instability of the metal alkoxides itself, especially in the presence of water and moisture, which makes it difficult to handle. As a result, alternative methods have been developed to employ metal salts instead of alkoxides in aqueous solution, together with small organic molecules as chelating agents, such as hydroxycarboxylic acids, to modify the hydrolysis chemistry of metal ions in aqueous solution.

One of the most commonly used organic acids is citric acid. Given its low price and wide availability, the sol–gel method with citric acid has been widely used to synthesize various metal oxides, including binary and tertiary oxides [105]. The key feature of this method is the formation of a metal-citrate complex, which ensures the homogeneity of the starting liquid solution. The presence of a citrate organic matrix is believed to help maintain the uniform mixing and dispersion of the metal ions on the atomic scale, resulting in small crystallite sizes.

A modification to the citrate sol–gel method was developed by Pechini in 1967 [106], where polyhydroxy alcohol, such as ethylene glycol, was added into the aqueous citrate solution. This results in a polyesterification reaction, which forms a covalent polymeric network that entraps metal ions [104], allowing two or more metals to be dispersed homogeneously throughout the network, as shown in Figure 14. The intermediate product here is a brittle solid, which is subsequently subjected to thermal treatment, e.g., calcination, to drive off organic components and obtain the final metal oxide powder [107].

Further variations and modifications have been made since Pechini's initial proposition. For example, Pechini suggested metal oxides, hydroxides, and carbonates as possible cation precursor choices, but due to a need to control the amount of organic material in the final product, as well as economic reasons, nitrate salts have been a popular choice. Addi-

tionally, a modified pathway that substitutes the polyhydroxy alcohol for water subverts the esterification step and forms a gel-like substance instead.

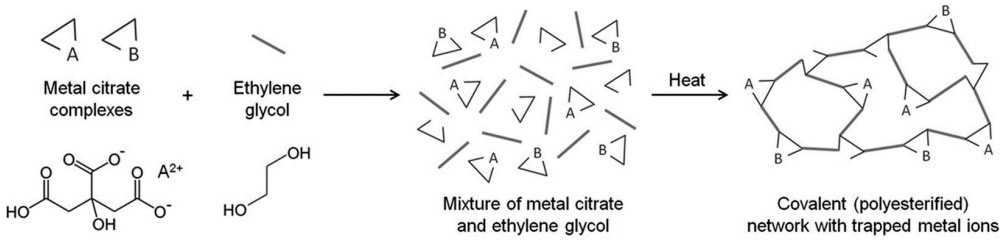

Figure 14. Formation of metal–organic gel via Pechini sol–gel synthetic method. Reprinted from ref. [104] with permission from the Royal Society of Chemistry.

Representative works on DFMs synthesized via a sol–gel method exhibit an expected degree of variability in terms of the synthetic pathways used. Nitrate precursors were common, though we note a study by Radfarnia et al. that used calcium acetate and aluminum isopropoxide as the metal cation precursors [108]. A study by Naeem et al. used ethylene glycol for polyesterification [69], as in the original Pechini method, while the aqueous citric acid variation is more common [109–111].

Notably, a study by Zhang et al. demonstrated that a sol–gel synthetic method produces DFMs with superior CO_2 capture capacities in comparison with other methods like co-precipitation and mixing [112]. Their study investigated the usage of CaO-based DFMs in the oxidative dehydrogenation of ethane. The sorbent component was comprised of ceria-doped CaO, which was synthesized via four methods—dry and wet mixing, co-precipitation, as well as the modified Pechini method with nitrate precursors of the calcium and cerium cations, and aqueous citric acid serving as the chelating agent. It was found that the sol–gel method produced a sample with an initial CO_2 capture capacity of 0.58 g/g, almost five times higher than that prepared by the dry mixing method, which exhibited an initial CO_2 capture capacity of 0.12 g/g. It was concluded that multiple factors influenced the CO_2 capturing abilities of a particular sorbent. While the available surface area is important, larger crystallite sizes severely impede the carbonation reaction when a surface layer of $CaCO_3$ forms around the sorbent material, causing the carbonation reaction to transit into the diffusion-controlled phase [52,54,55]. Therefore, a balance between maximizing the surface area and optimizing the crystallite sizes is necessary for ensuring excellent CO_2 capturing capacities, which can be obtained by fine-tuning the sol–gel synthesis parameters.

4.3. Co-Precipitation Method

Co-precipitation is a widely employed method in heterogeneous catalysis to synthesize materials such as mixed metal oxides [113,114]. The general method involves dissolving the precursor chemicals for the adsorbent, catalyst, and/or support/promoter (typically nitrate salts) in either deionized water or polar solvent under rigorous stirring to ensure homogeneity. A precipitating agent, e.g., NaOH, NH_4OH, etc., is then added dropwise to induce precipitation. Subsequently, aging to enhance crystallinity is practiced, though not necessary. The precipitate is collected via filtration followed by washing cycles in deionized water or another solvent. Lastly, the precipitate is subjected to thermal treatment, e.g., calcination, to obtain the final product.

As a synthetic method, co-precipitation is straightforward and inexpensive. The material's stoichiometry can be easily controlled by using appropriate amounts of precursors during the precipitation reaction. Depending on the aging conditions, adsorbents produced via this method typically exhibit a homogeneous particulate distribution with good crystallite sizes. However, disadvantages of this method include generally lower surface areas compared to adsorbents synthesized via IWI or sol–gel methods [105]. The process is also fairly laborious, with repeated washing being commonly necessary. Further, Li et al.

note that the structural properties of the resulting precipitate are sensitive and heavily dependent on reaction conditions and equipment setup, which makes reproducibility an issue [115].

Like the sol–gel pathways, there are several variations to the co-precipitation procedure. These include the types of precipitating agent, the solvent used to dissolve the precursors and wash the precipitate, any mechanical assistance to the reaction (e.g., stirring, sonication, microwave, etc.), as well as aging temperature and time, to enhance the crystallinity via Ostwald ripening [114,115] at a high temperature, e.g., hydrothermal treatment. With the careful selection and optimization of the reaction conditions, the wide variation of methods under the family of co-precipitation procedures could be used to overcome certain shortcomings or to reinforce certain desirable qualities in a DFM. For example, Molina-Ramírez et al. synthesized a DFM comprising of a Ni-Ba unsupported catalyst via a co-precipitation method assisted by sonication [116], where nitrate precursors were used and ammonia was employed as the precipitant. The as-synthesized DFM showed an exceptionally high BET surface area of 112 m^2/g, though we note that colloidal silica was used as a surface area promoter. Meanwhile, Karami and Mahinpey investigated the effect of synthetic methods on several Ca-alumina sorbents [117], such as the precipitation of a Ca salt solution onto colloidal gelled alumina, the co-precipitation of Ca and Al salt solutions with Na_2CO_3 or sodium aluminate as the precipitants, and the physical mixing of a Ca precipitate with a peptized alumina gel. It was found that co-precipitation produced a sorbent with the poorest CO_2 uptake performance, possibly due to the low surface area and porosity.

4.4. Mixing Method

The mixing of adsorbent/catalytic/support precursors under varying conditions to produce a DFM precursor is arguably the simplest and most straightforward synthetic method. However, it clearly lacks precision in terms of producing the most favorable microstructures required for the ICCC process. Slightly varied methods of mixing exist depending on the relative solubilities of the precursors used [53]. For example, the wide usage of nitrate precursors as described in the preceding sections lends itself to facile dissolution in water. The precursor solutions are then simply mixed under stirring for a few hours to ensure homogeneity, the resultant solution is then dried to obtain a powder, followed by calcination to obtain the DFM.

Mixing is more commonly used in conjunction with other synthetic methods to produce a DFM. For example, the adsorbent component might be synthesized by mixing, while the catalytic component is synthesized via another method, e.g., co-precipitation or impregnation. For example, in a work by Huang et al., who investigated the performance of $NaNO_3$-promoted Ni/MgO DFMs for integrated CO_2 capture and methanation, the unpromoted Ni/MgO catalysts were synthesized via a facile one-pot wet mixing method [118], whereas the alkali metal salt promoter $NaNO_3$ was subsequently impregnated upon the bare catalyst. When mixing is employed as the sole synthetic method for a DFM, its characteristics are decidedly inferior. Wu et al. demonstrated this in a comparative study investigating the use of Ni-CaO-CeO_2 DFMs for ICCC via the RWGS reaction [105]. Different DFMs were prepared using acetate/nitrate precursors of Ni, Ca, and Ce via wet mixing, co-precipitation, and sol–gel methods. It was found that the wet mixing method produced a sample with the lowest CO_2 capture capacity and product yield as compared to the other synthetic methods. The poor performance by wet mixing is mainly due to the low BET surface area, inferior pore structure, large Ni crystallite sizes, low surface basicity, and low reducibility.

5. Performance Evaluation of Dual Function Materials

With a general understanding of the kinetics and thermodynamics of CO_2 capture and conversion, as well as the typical synthetic methods of DFMs that enable the ICCC process, we proceed to evaluate the performance of DFMs across the literature. This section catalogues recent works according to the key ICCC reactions that the DFM catalyzes, namely

ICCC with a methanation reaction, a reverse water–gas shift (RWGS) reaction, and the dry reforming of methane (DRM). With each case study, we present examples of the synthetic, operating, and performance parameters of the DFMs, as well as the characteristics and mechanistic studies of the interaction between CO_2 and the adsorption and catalytic sites of the DFMs. Given the dual function characteristic of the materials, the efficacy of DFMs first depends on their ability to efficiently capture CO_2 with a high capacity, which becomes the reactant for the subsequent reactions. Therefore, the material selection for a DFM has to satisfy the specific operating conditions required for both CO_2 capture and reaction. As DFMs are subjected to repeated cycles of CO_2 capture and reaction, the robustness of the materials is also an important factor to be considered in the design and evaluation of DFMs.

5.1. ICCC with Methanation Reaction

The majority of studies on ICCC using DFMs focus on the methanation of CO_2, which takes place primarily via the Sabatier reaction (Equation (9)):

$$CO_2 + 4H_2 \rightleftarrows CH_4 + 2H_2O \Delta H_R = -165 \frac{kJ}{mol} \quad (9)$$

The reaction is typically carried out at temperatures around 300–350 °C and pressures of 5–20 MPa [119]. Given its highly exothermic nature, the reaction releases copious amounts of heat, which has to be managed accordingly to prevent the thermal degradation (e.g., sintering) of the DFMs. This can be achieved via the engineering of more thermally resistant DFMs, or by harnessing the heat of the reaction via efficient heat transfer and heat integration, e.g., powering endothermic reactions. In this view, CO_2 methanation offers an isothermal solution to the DFMs system because the exothermic reaction can supply the required heat for the decarbonation reaction. Additionally, the usage of real flue gas in industrial settings might lead to the poisoning and deactivation of the Ni-based DFMs typically used for methanation [119,120]. Practical solutions include the pre-scrubbing of the flue gas or considering the usage of alternative catalysts like Ru, which can be activated via pre-reduction at lower temperatures in a H_2 environment. The vast body of work studying the ICCC–methanation process is summarized in Table 3. It can be seen that Ru- and Ni-based DFMs supported on alkaline metal oxides, such as Na_2O, MgO, and CaO, are the most commonly studied materials. In fact, as shown in Figure 15, Na_2O, MgO, and CaO are among the most common sorbents for ICCC with methanation [14], due to their high CO_2 sorption capacity and methanation activity at moderate temperatures, given the thermodynamic limitation of the reaction.

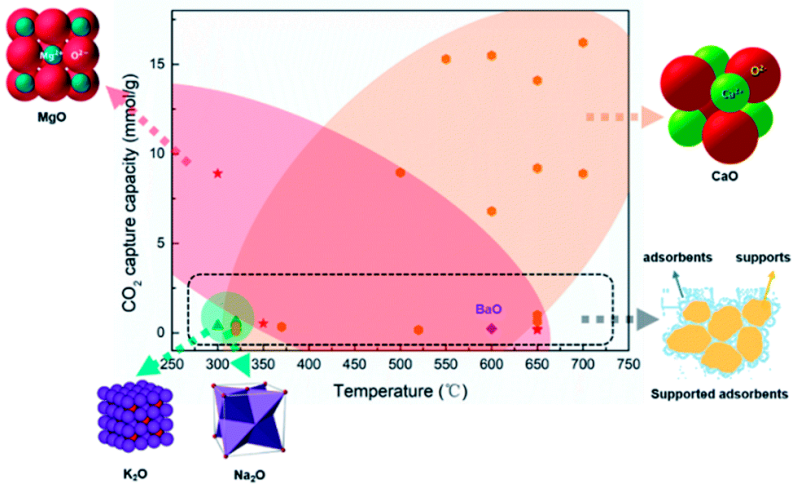

Figure 15. Typical CO_2 adsorption capacity of DFMs for ICCC–methanation. Orange zone: CaO; Red zone: MgO; Green zone: K_2O and Na_2O. Reprinted from ref. [14] with permission from the Royal Society of Chemistry.

Table 3. Literature summary of DFMs that catalyze the methanation reaction.

DFM	Synthesis Method	Carbonation Conditions	Methanation Conditions	CO_2 Sorption Capacity (mmol/g)	CO_2 Conversion (%)	Methanation Capacity (mmol/g)	Ref.
5% Ru 10% CaO/Al_2O_3	IWI	320 °C, 10%CO_2/air	320 °C, 5%H_2/N_2	0.41	76.17%	0.31	[11]
5% Ru 10% CaO/Al_2O_3	IWI	320 °C, 10%CO_2/N_2	320 °C, 4%H_2/N_2	-	-	0.5	[93]
5% Ru 10% K_2CO_3/Al_2O_3	IWI	320 °C, 10%CO_2/N_2	320 °C, 4%H_2/N_2	-	-	0.91	[93]
5% Ru 10% Na_2CO_3/Al_2O_3	IWI	320 °C, 10%CO_2/N_2	320 °C, 4%H_2/N_2	-	-	1.05	[93]
5% Ru 6.1% Na_2O/γ-Al_2O_3	IWI	300 °C, simulated flue gas	300 °C, 15%H_2/N_2	0.4 (50-cycle average)	77%	0.32	[98]
5% Ru-6.1% "Na_2O"/Al_2O_3	IWI	320 °C, 10%CO_2/N_2	320 °C, 10%H_2/N_2	0.651	96%	0.614	[92]
0.5% Rh-6.1% "Na_2O"/Al_2O_3	IWI	320 °C, 10%CO_2/N_2	320 °C, 10%H_2/N_2	0.626	69%	0.422	[92]
15% Ni 15% CaO/Al_2O_3	IWI	280–520 °C, 10%CO_2/Ar	280–520 °C, 10%H_2/Ar	-	-	0.142	[101]
15% Ni 10% Na_2CO_3/Al_2O_3	IWI	280–520 °C, 10%CO_2/Ar	280–520 °C, 10%H_2/Ar	-	-	0.186	[101]
4% Ru 10% CaO/Al_2O_3	IWI	370 °C, 1.4%CO_2/Ar	370 °C, 10%H_2/Ar	0.253	-	0.272	[96]
4% Ru 10% Na_2CO_3/Al_2O_3	IWI	370 °C, 1.4%CO_2/Ar	370 °C, 10%H_2/Ar	0.391	-	0.398	[96]
1% Ru, 10% Ni, 6.1% "Na_2O"/Al_2O_3	IWI	320 °C, 7.5%CO_2-4.5%O_2-15%H_2O-balance N_2	320 °C, 15%H_2/N_2	0.52 (3-cycle average)	81% (3-cycle average)	0.38 (3-cycle average)	[100]
1% Ru, 10% Ni, 6.1% "Na_2O"/Al_2O_3	IWI	320 °C, 7.5%CO_2-4.5%O_2-15%H_2O-balance N_2	320 °C, 15%H_2/N_2	0.52 (20-cycle average)	100% (20-cycle average)	0.38 (20-cycle average)	[100]
1% Pt 10% Ni 6.1% "Na_2O"/Al_2O_3	IWI	320 °C, 7.5%CO_2-4.5%O_2-15%H_2O-balance N_2	320 °C, 15%H_2/N_2	0.35 (3-cycle average)	87% (3-cycle average)	0.25 (3-cycle average)	[100]
2.5Ru/CeO_2-MgO	Impregnation/physical mixing	300 °C, 65%CO_2/N_2	300 °C, 5%H_2/N_2	-	60% (1st cycle); 39% (10th cycle)	5.73 (1st cycle); 1.13 (10th cycle)	[121]
5Ru/CeO_2-MgO	Impregnation/physical mixing	300 °C, 65%CO_2/N_2	300 °C, 5%H_2/N_2	-	74% (1st cycle); 79% (10th cycle)	6.6 (1st cycle); 3.36 (10th cycle)	[121]

Table 3. *Cont.*

DFM	Synthesis Method	Carbonation Conditions	Methanation Conditions	CO_2 Sorption Capacity (mmol/g)	CO_2 Conversion (%)	Methanation Capacity (mmol/g)	Ref.
10Ru/CeO_2-MgO	Impregnation/physical mixing	300 °C, 65%CO_2/N_2	300 °C, 5%H_2/N_2	-	89% (1st cycle); 69% (10th cycle)	7.07 (1st cycle); 2.31 (10th cycle)	[121]
Ni/Na-γ-Al_2O_3	IWI	450 °C, 5%CO_2/N_2	450 °C, H_2	0.209	96%	0.188	[122]
Ni/Na-γ-Al_2O_3	IWI	450 °C, 5%CO_2/N_2	450 °C, H_2	0.299	92%	0.266	[122]
0.95% Ru-5% K/Al_2O_3	IWI	350 °C, 2.5%H_2O/3%O_2/1%CO_2/He	350 °C, 4%H_2/He	0.028 (3rd cycle)	-	0.028 (3rd cycle)	[123]
0.95% Ru-5.1% Ca/Al_2O_3	IWI	350 °C, 2.5%H_2O/3%O_2/1%CO_2/He	350 °C, 4%H_2/He	0.116 (3rd cycle)	-	0.036 (3rd cycle)	[123]
0.84% Ru-16% Ba/Al_2O_3	IWI	350 °C, 2.5%H_2O/3%O_2/1%CO_2/He	350 °C, 4%H_2/He	0.165 (3rd cycle)	-	0.080 (3rd cycle)	[123]
0.5% Ru, 6.1% "Na_2O"/Al_2O_3	IWI	320 °C, 400 ppm CO_2/air	320 °C, 15% H_2/N_2	0.2	-	0.15	[124]
1%Ni/CeCaO-imp	One-pot citric acid chelation/wet impregnation	550 °C, 15%CO_2/N_2	550 °C, H_2	10.6	42%	3.3	[125]
1%Ni/CeCaCO_3-imp	One-pot citric acid chelation/carbonation/wet impregnation	550 °C, 15%CO_2/N_2	550 °C, H_2	14.1	52%	6	[125]
1%Ni/CeO_2-CaO-phy	Hydrothermal/one-pot citric acid chelation/physical mixing	550 °C, 15%CO_2/N_2	550 °C, H_2	15.3	62%	8	[125]
Ru-BaO/Al_2O_3 (intimate mixture)	IWI	350 °C, 1%CO_2/He	350 °C, 4%H_2/He	0.025	20% at 291 °C	0.151	[126]
BaO/Al_2O_3 + Ru/Al_2O_3 (mechanical mixture)	IWI	350 °C, 1%CO_2/He	350 °C, 4%H_2/He	0.055	20% at 362 °C	0.097	[126]
5Li-Ru/A	IWI	263 °C, 10%CO_2/N_2	263 °C, 10%H_2/N_2	-	98%	0.32	[127]
5Li-Ru/A	IWI	293 °C, 10%CO_2/N_2	293 °C, 10%H_2/N_2	-	97.4%	0.34	[127]
5Li-Ru/A	IWI	318 °C, 10%CO_2/N_2	318 °C, 10%H_2/N_2	-	95.4%	0.29	[127]
30% $LaNiO_3$/CeO_2	Citric acid/impregnation	400 °C, 1.4%CO_2/Ar,	400 °C, 10%H_2/Ar	0.089 (3-cycle average)	-	0.08 (3-cycle average)	[128]

Table 3. *Cont.*

DFM	Synthesis Method	Carbonation Conditions	Methanation Conditions	CO_2 Sorption Capacity (mmol/g)	CO_2 Conversion (%)	Methanation Capacity (mmol/g)	Ref.
AMS/CaMgO||Ni1-Co3	Sol–gel/solvent evaporation	350 °C, 95%CO_2/N_2	350 °C, 10%H_2/N_2	14.7 (sorbent mass basis)	76.4%	5.46 (catalyst mass basis)	[129]
AMS/CaMgO||Ni1-Co1	Sol–gel/solvent evaporation	350 °C, 95%CO_2/N_2	350 °C, 10%H_2/N_2	14.4 (sorbent mass basis)	90%	9.97 (catalyst mass basis)	[129]
AMS/CaMgO||Ni3-Co1	Sol–gel/solvent evaporation	350 °C, 95%CO_2/N_2	350 °C, 10%H_2/N_2	14.1 (sorbent mass basis)	75%	6.66 (catalyst mass basis)	[129]
cDFM-2-0.4Ni-10Cs	Co-precipitation/IWI	350 °C, 15%CO_2/N_2	350 °C, H_2	0.48	-	0.33	[130]
20% $LaNiO_3$/CeO_2	Citric acid/impregnation	480 °C, 10%CO_2/Ar	480 °C, 10% H_2/Ar	0.113	-	0.075	[131]
20% La0.5Ca0.5NiO_3/CeO_2	Citric acid/impregnation	480 °C, 10%CO_2/Ar	480 °C, 10% H_2/Ar	0.175	-	0.140	[131]
Ni/CaZrO	Sol–gel	600 °C, 15%CO_2/N_2	600 °C, 66.7%H_2/N_2	9.9–9 (20 cycles)	86.3–78% (20 cycles)	6.7 (6th to 20th cycle)	[110]
NiO-MgO	Co-precipitation	320 °C 10%CO_2/5%O_2/He	320 °C, 20%H_2/He	~0.3 (10 cycles)	~96% (10 cycles)	~0.26 (10 cycles)	[132]
Cs-impregnated Ni-MgO-Al_2O_3 extrudate (EI)	Co-precipitation/ impregnation	350 °C, 15%CO_2/N_2	350 °C, H_2	0.24	75% (250h on-stream)	0.18 (250h on-stream)	[133]

IWI: incipient wetness impregnation.

With a wide range of variables that are at play in the synthesis of a DFM, an extensive amount of work is naturally devoted to finding the best synthetic routes that produce DFMs with optimized makeups [11,95,101,110,117,121–123,125–131,134–136]. In a pioneering work by Duyar et al., CaO-based DFMs with Ru as the methanation catalyst supported on alumina were synthesized via incipient wetness impregnation (IWI) with varying adsorbent/catalyst loadings [11]. It was observed that the order of impregnation (i.e., Ru impregnated on CaO-alumina vs. CaO impregnated on Ru-alumina) affected the CO_2 capture and methanation performances at 320 °C. In particular, a DFM comprising 5 wt% Ru impregnated on 10 wt% CaO-γAl_2O_3 showed a single-pass methanation capacity of 0.5 mmol/g. Upon subjecting to cyclic testing, an average of 0.41 mmol/g of CO_2 capture could be obtained, with an average CO_2 conversion of 76.17% and a methanation capacity of 0.31 mmol CH_4/g over 19 cycles. The authors concluded that the order of impregnation was significant where the impregnation of Ru was found to be better than that of CaO due to the good dispersion of Ru. Should the order be reversed, the active Ru sites could be blocked by CaO particles, thus decreasing the catalytic activity of the DFM. Upon varying the CaO:Ru ratio, a high methane turnover (CH_4 yield/Ru) was observed at a high CaO:Ru ratio, indicating CO_2 spillover from the CaO to Ru sites where the methanation reaction takes place. It also suggests that the close proximity of CaO and Ru was an important factor in the DFM performance. However, low Ru loadings might not generate enough heat from the exothermic methanation reaction to liberate CO_2 chemisorbed to CaO, since methanation begins primarily where CO_2 is chemisorbed to Ru, thus compromising the overall CH_4 yield. Lastly, testing under simulated flue gas conditions showed that, in the presence of steam, the methanation capacity decreased to 0.27 mmol CH_4/g over 20 cycles, although the purity of the effluent gas improved to 99.9% CH_4 by volume, as compared to 83.6% CH_4 (balance CO_2) in the absence of steam, suggesting the competing adsorption of H_2O and CO_2 on the DFM surface. A follow-up study by Duyar et al. presented two new DFMs with similar adsorbent/catalyst loadings, but with K_2CO_3 or Na_2CO_3 substituting CaO as the adsorbent component [93]. These DFMs showed improved methanation capacities of 0.91 and 1.05 mmol CH_4/g for K and Na, respectively, owing to the increasing CO_2 adsorption capacity in the same order: Na_2CO_3 > K_2CO_3 > CaO. The results, therefore, show the importance of optimizing the adsorbent component of DFMs in future attempts to engineer more efficient materials.

In another study, Porta et al. assessed the CO_2 capture and methanation performances at 350 °C of Ru-based DFMs with six different adsorbent components (Li/Na/K/Mg/Ca/Ba) supported on alumina [123]. They found that metals capable of forming carbonates with high thermal stability led to the production of the highest amounts of CH_4, namely, DFMs promoted with K, Ca, and Ba. On the other hand, Arellano-Treviño et al. evaluated Ru-based DFMs supported on γ-Al_2O_3 containing different alkali and alkaline earth oxides, such as Na_2O, K_2O, CaO, and MgO, and found that Na_2O-promoted DFM (5%Ru-6.1%Na_2O/Al_2O_3) exhibited a high CO_2 capture capacity (0.651 mmol/g) and methanation rate (0.614 mmol CH_4/g) when tested in 10%CO_2/N_2 atmosphere [92]. Although the CH_4 yield significantly decreased upon exposure to a simulated flue gas condition (7.5%CO_2, 4.5%O_2, 15%H_2O, balance N_2), the DFM remained active, producing 0.291 mmol CH_4/g at 320 °C. In another experiment using a Rh-Na_2O-based DFM, the CO_2 capture capacity and catalytic activity of 0.5%Rh was compared with those of 5%Ru in order to obtain a similar material price. While both DFMs exhibited a similar CO_2 capture capacity (0.625 vs. 0.651 mmol/g, respectively), 5%Ru yielded higher methanation (0.614 mmol/g) than the 0.5%Rh counterpart (0.422 mmol/g), although one could argue that the methane yield per unit of metal is higher for Rh than that for Ru. As an alternative to noble metals, Ni-Na_2O-based DFM was also synthesized and tested, which produced 0.276 mmol CH4/g under a 10%CO_2/N_2 atmosphere. However, the material was deactivated when exposed to flue gas containing H_2O, with no methane being produced, as shown in Figure 16. Further analysis suggested that Ni atoms could not be completely reduced to the active metallic state in the presence of O_2 and H_2O, thus losing its catalytic activity.

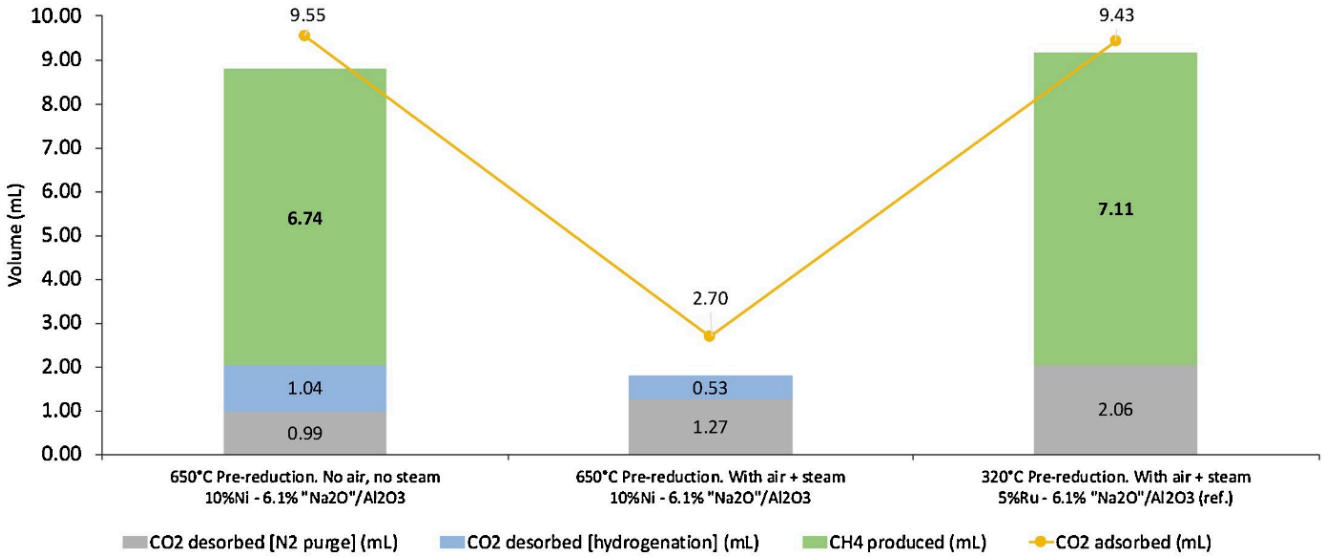

Figure 16. CO_2 adsorption, desorption, and CH_4 produced on 10%Ni-6.1%"Na_2O"/Al_2O_3 with and without O_2 and steam present in the CO_2 feed. CO_2 capture and methanation were performed at 320 °C, 1 atm. Reprinted from ref. [92] with permission from Elsevier.

Further possible variables during the synthesis of a DFM include the choice of adding promoters that can improve the CO_2 capture capacity and CH_4 selectivity, or the choice of precursor chemicals, which might affect the interactions between different components in the synthesized DFM. One study by Cimino et al. [135] found that promoting Ru/Al DFM with Li resulted in a four-to-five-fold increase in the CO_2 capture capacity compared to the unpromoted material. In addition, stable cyclic carbonation/methanation was possible at temperatures around 230 °C, instead of the commonly utilized temperatures of 300 to 320 °C. In another study, the incorporation of Cs into Ni-hydrotalcite-based DFMs was found to increase the CO_2 capture capacity up to 0.48 mmol/g and a CH_4 yield of 0.33 mmol/g at 350 °C [130]. These examples show the promotional effect of alkali metal as it increases the material's basicity, in particular, the number of medium and strong basic sites. Besides enhancing the basicity of the material, the addition of a promoter can also improve the stability of the material. For example, Ma et al. investigated the effect of doping Ni-CaO-based DFMs with various metal oxides, such as Mg, Al, Mn, Y, Zr, La, and Ce [110]. Among the synthesized DFMs, Zr-doped Ni/CaO exhibited the best performance by maintaining a stable CO_2 capture capacity of 9 mmol/g and 74% CH_4 selectivity after 20 cycles. It was attributed to the formation of $CaZrO_3$, which helped improve the thermal resistance to sintering.

To investigate the effect of catalyst loading, Bermejo-López et al. varied the Ni content on CaO- or Na_2CO_3-based DFMs with alumina support through the impregnation method [101]. Notably, it was found that increasing Ni loading would increase the particulate sizes, catalyst reducibility, and consequently, methanation rates, with 0.142 mmol CH_4/g produced by a DFM comprising 15 wt% Ni on 15% CaO/Al_2O_3 at 520 °C.

Lastly, the choice of the synthetic method has also been known to significantly influence the final microstructures and other physicochemical characteristics of a DFM, and a range of works have been devoted to comparatively evaluating the various possible synthetic routes [105,112,117,125]. For example, Zhang et al. noted that sol–gel synthetic methods tend to produce DFMs with physicochemical characteristics more favorable for ICCC processes, including an optimal balance of the BET surface area and crystallite sizes [112]. Sun et al. noted that the dispersion between catalyst and sorbent particles could even be tuned via different synthetic methods, thus giving rise to varying carbonation and methanation capabilities [125].

In addition to optimizing the materials design and synthesis, careful attention should also be given to the experimental parameters of the carbonation and methanation reaction, as well as the simulated flue gas conditions, as they can help uncover the possibility of translating ideal laboratorial conditions to a more real-life (e.g., industrial) setting, and provide plausible avenues for future work [98,100,122,124,137]. In one such study by Wang et al., a DFM consisting of Ru-Na_2O impregnated on an alumina support was subjected to parametric and cyclic tests [98]. Specifically, the effect of three parameters—gas space velocity, reaction temperature, and exposure to oxygen during adsorption—on performance indicators such as CO_2 uptake and CH_4 generation, were investigated. From the cyclic studies, a CO_2 uptake and CH_4 generation capacities of 0.40 mmol/g and 0.32 mmol/g, respectively, were reported after 50 cycles at 300 °C. Through parametric studies, it was found that gas space velocities and temperature would affect the rates and the extents of carbonation and methanation in accordance with kinetic and thermodynamic principles. For instance, increasing the gas space velocity would increase the rates of CO_2 uptake and CH_4 production due to a more efficient mass transfer, whereas increasing the temperature would decrease CO_2 adsorption and CH_4 generation due to the exothermic nature of the reactions. The oxygen exposure tests also showed that, minimally, 15% H_2/N_2 for methanation was necessary for the reduction of oxidized Ru due to exposure to oxygen-containing flue gas during adsorption. The presence of precious metals such as Ru in overcoming the limitations of Ni as a catalytic metal is further displayed by studies such as one by Arellano-Treviño et al., which suggests that Ru doping aids in the reduction and re-activation of Ni after oxygen exposure, leading to the possibility of developing DFMs which are more resistant to industrial reaction conditions at cheaper costs [100].

Meanwhile, other authors have studied reaction parameters such as optimal carbonation/methanation durations, feed gas concentrations, and process pressures. Kosaka et al., for example, investigated Ni-based DFMs promoted with alkali metals including Na/K/Ca supported on alumina for their carbonation and methanation at 450 °C [122]. It was found that increasing operational pressures (a range of 0.1 MPa to 0.9 MPa was used) could increase the CO_2 capture capacity of a Ni/Na-Al_2O_3 DFM from 0.209 mmol CO_2/g to 0.299 mmol CO_2/g, and its methanation capacity from 0.188 mmol CH_4/g to 0.266 mmol CH_4/g, in agreement with thermodynamics as the methanation reaction involves a decrease in the number of moles. For these tests, a gas feed containing 5% CO_2/N_2 was used, but it was additionally reported that increasing pressures enhanced carbonation and methanation at lower CO_2 concentrations of 100 and 400 ppm CO_2/N_2 as well. Jeong-Potter and Farrauto also attempted an investigation of the effectiveness of a Ru/Na-Al_2O_3 DFM at a CO_2 concentration of 400 ppm in air to assess the feasibility of utilizing the DFM for direct air capture purposes [124].

Considering that ICCC and methanation have been extensively studied, a good understanding of the kinetics and mechanisms of carbonation and methanation is equally important [94–96,138–140]. The mechanistic study is typically performed via investigative techniques including Fourier transform–infrared (FT-IR) spectroscopy, which is capable of measuring the gas composition at the reactor outlet and its changes with time, or by in situ diffuse reflectance infrared Fourier transform spectroscopy (DRIFTS), which detects the presence of chemical bonds that suggest the occurrence of possible reaction intermediates.

For instance, a study by Bermejo-López et al. uses FT-IR to study the temporal evolution of the gas composition within a reactor [96]. Their work involved the usage of Ru-based CaO and Na_2CO_3 DFMs supported on alumina. They proposed a mechanism where $CaCO_3$ formed through the carbonation of $Ca(OH)_2$ (Equations (10) and (11)) is decomposed upon the addition of H_2 during the methanation step (Equation (12)), releasing CO_2 which is subsequently converted on Ru sites according to the Sabatier reaction (Equation (13)). Additional observations include the delayed evolution of CO_2 itself during the carbonation step, suggesting the saturation of the CO_2 uptake sites, and the delayed evolution of H_2O during methanation (even though the Sabatier reaction produces H_2O), suggesting the

hydration of CaO to form $Ca(OH)_2$ (Equation (14)). A similar reaction scheme is suggested for Na_2CO_3-based DFMs.

$$CaO + CO_2 \leftrightarrow CaCO_3 \quad (10)$$

$$Ca(OH)_2 + CO_2 \leftrightarrow CaCO_3 + H_2O \quad (11)$$

$$CaCO_3 \leftrightarrow CaO + CO_2 \quad (12)$$

$$CO_2 + 4H_2 \leftrightarrow CH_4 + 2H_2O \quad (13)$$

$$CaO + H_2O \leftrightarrow Ca(OH)_2 \quad (14)$$

Conversely, other studies utilize DRIFTS to detect the presence of reaction intermediates, and suggest possible reaction mechanisms [94,95,140]. One such study by Proaño et al. with Ru-based DFM [94,95] suggests the formation of bidentate carbonate species during carbonation and formate species during methanation (see Figure 17 for their detailed mechanism), but there exists a range of works that find corroborating [139] and disputing [140] results. Proaño's group has since conducted further studies into DFMs with a similar makeup (10% Ni, 6.1% Na_2O/Al_2O_3 DFMs enhanced with 1% Pt/Ru), utilizing in situ DRIFTS to study carbonation and methanation under oxidizing and non-oxidizing conditions, yielding largely corroborative results.

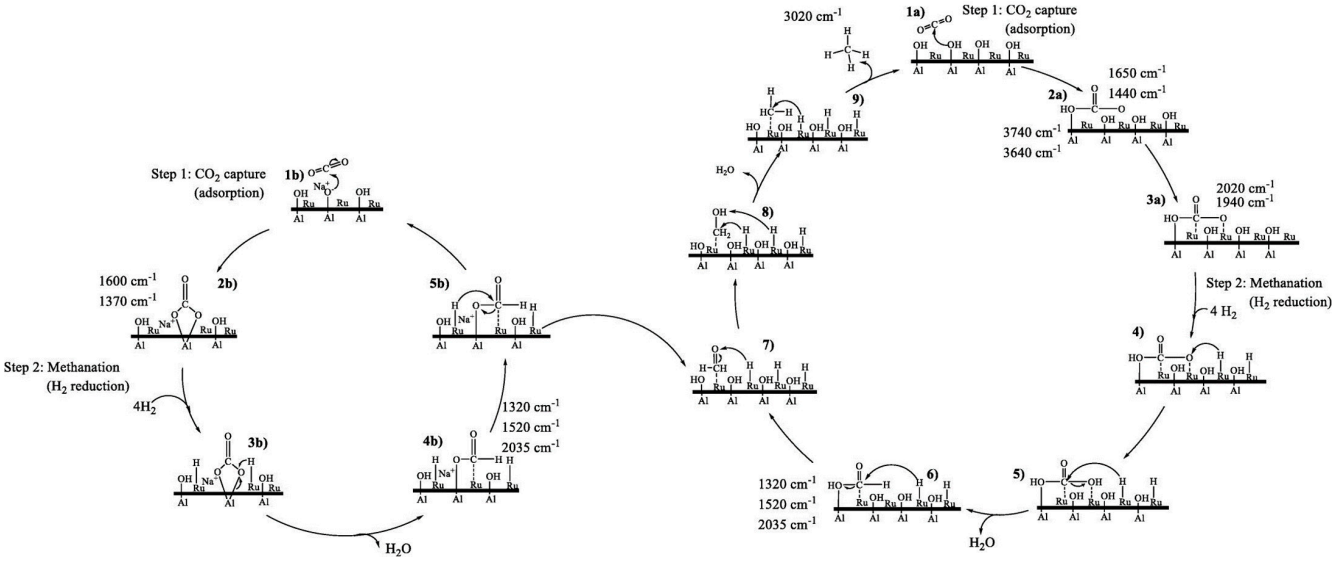

Figure 17. Proposed carbonation and methanation mechanisms for 5%Ru/Al_2O_3 (right) and 5%Ru-6.1%"Na_2O"/Al_2O_3 DFMs (left to right). Reprinted from ref. [95] with permission from Elsevier.

5.2. ICCC with Reverse Water–Gas Shift (RWGS) Reaction

RWGS is another key reaction in C1 chemistry that takes place according to the following reversible reaction (Equation (15)):

$$CO_2 + H_2 \rightleftarrows CO + H_2O; \Delta H_R = 41.2 \frac{kJ}{mol} \quad (15)$$

RWGS is an important reaction for producing syngas with desired H_2/CO ratios, where CO can be further valorized into various chemicals, such as methanol via the CAMERE (carbon dioxide hydrogenation to form methanol via a reverse-water–gas-shift reaction) process or hydrocarbons via Fischer–Tropsch synthesis. However, although CO is industrially more useful than methane, the development of an effective DFM system to generate CO has been much less explored than that for methane generation. This is

partly because the ability of DFMs to achieve a practical H_2/CO ratio remains a major challenge. The accurate tuning of syngas composition can be tricky because of other secondary reactions that may occur in parallel with the RWGS reaction, such as the Sabatier reaction (Equation (10)) and the methanation of CO (Equation (16)):

$$CO + 3H_2 \rightleftarrows CH_4 + H_2O; \Delta H_R = -206 \frac{kJ}{mol} \quad (16)$$

Considering the endothermic nature of RWGS, increasing operating temperatures might reduce the extent of the exothermic side reactions and favor the RWGS reaction. Indeed, in a review by González-Castaño et al. [141], where the equilibrium concentrations of chemical species involved in the RWGS, Sabatier, and CO methanation reactions were investigated, it was found that the equilibrium concentration of CH_4 decreases to near zero above 700 °C, as shown in Figure 18. In addition, the CO_2/H_2 molar ratio also plays a critical role in adjusting the CO composition, with a low CO_2/H_2 ratio being thermodynamically favorable for the RWGS reaction. These considerations are therefore important in maximizing the selectivity of CO, which turns out to be a key metric in evaluating DFMs used in ICCC processes involving RWGS.

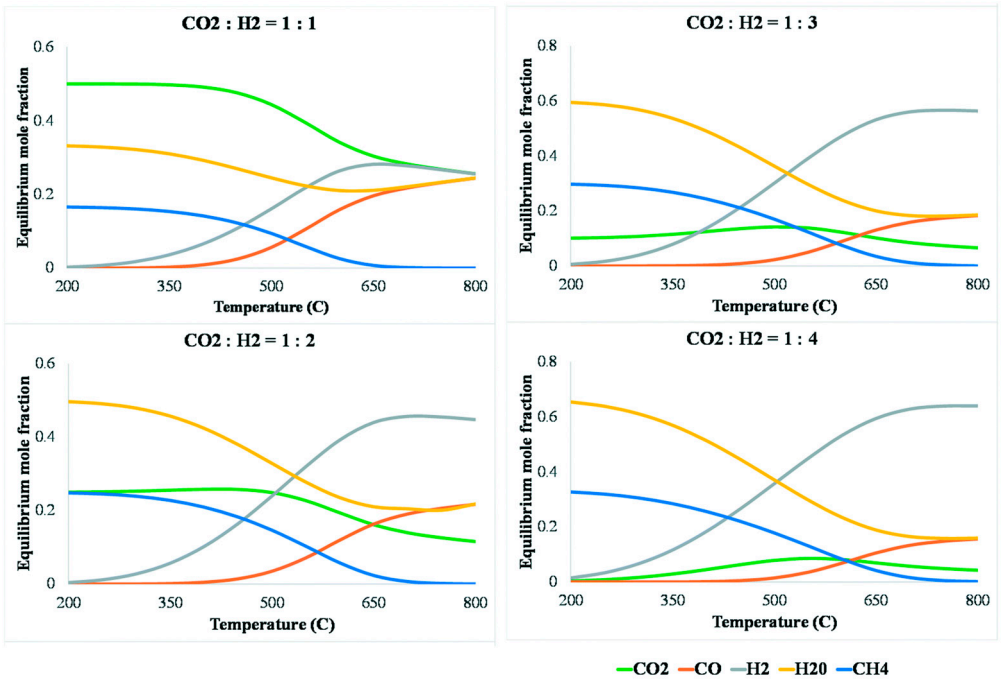

Figure 18. Equilibrium mole fractions of chemical species involved in the RWGS and its side reactions. Reprinted from ref. [141] with permission from the Royal Society of Chemistry.

Apart from thermodynamic considerations, ensuring a high selectivity of CO is also dependent on a prudent catalyst design, which is aided by the understanding of the kinetics and mechanisms of RWGS. Conventionally, Cu is favored for its CO selectivity and low methanation rates, while Pt is preferred for higher CO_2 conversions [78]. With regards to DFM selection for the RWGS reaction, a variety of materials have been developed, including those containing transition metals, such as Fe, Co, Ni, or combinations thereof [142,143]. Recently, there have also been studies that do not involve any transition metals, such as supported Na on CaO and Al_2O_3 [144,145]. Table 4 summarizes the DFMs that catalyze the RWGS reaction.

Table 4. Literature summary of DFMs that catalyze the RWGS reaction.

DFM	Synthesis Method	Carbonation Conditions	RWGS Conditions	CO_2 Sorption Capacity (mmol/g)	CO_2 Conversion (%)	Recycle Study and CO Yield Loss	Ref.
Ni-CaO-CeO_2 (CP)	Co-precipitation with acetate precursors	650 °C, 10% CO_2/N_2	650 °C, 10% H_2/N_2	9.81	75	10 cycles, ~10% loss	[105]
Ni-CaO-CeO_2 (WM)	Wet mixing with acetate precursors	650 °C, 10% CO_2/N_2	650 °C, 10% H_2/N_2	8.54	84	10 cycles, stable	[105]
Ni-CaO-CeO_2 (SG-A)	Citric acid-based sol–gel with acetate precursors	650 °C, 10% CO_2/N_2	650 °C, 10% H_2/N_2	15.34	92	10 cycles, 11.6% loss	[105]
Ni-CaO-CeO_2 (SG-N)	Citric acid-based sol–gel with nitrate precursors	650 °C, 10% CO_2/N_2	650 °C, 10% H_2/N_2	13.15	96	10 cycles, 3.5% loss	[105]
Ce-doped Ni/CaO ($Ca_1Ni_{0.1}Ce_{0.033}$)	Citric acid-based sol–gel with nitrate precursors	650 °C, 15% CO_2/N_2	650 °C, 5% H_2/N_2	14.1	51.8	20 cycles, stable	[111]
Ni-CaO-ZrO_2-12	Citric acid-based sol–gel with nitrate precursors	650 °C, 10% CO_2/N_2	650 °C, 45% H_2/N_2	16.72	63.2	12 cycles, 18.6% loss	[146]
Ni-CaO-6ZrO_2-6CeO_2	Citric acid-based sol–gel with nitrate precursors	650 °C, 10% CO_2/N_2	650 °C, 45% H_2/N_2	11.88	72.1	12 cycles, 12% loss	[146]
Ni/CeO_2-CaO	Physical mixing	650 °C, 20% CO_2/N_2	650 °C, 5% H_2/N_2	9.58	56.1	20 cycles, <5% loss	[147]
Na/Al_2O_3	Wetness impregnation	500 °C, 5% CO_2/N_2	500 °C, H_2	0.135	76.9	50 cycles at 450 °C, stable	[144]
Na/Al_2O_3	Wetness impregnation	500 °C, 400 ppm CO_2/N_2	500 °C, H_2	0.0907	77.7	-	[144]
Na-Pt/Al_2O_3	Wetness impregnation	350 °C, 1% CO_2/10% O_2/N_2	350 °C, 5% H_2/N_2	0.19	89	6000 cycles, stable	[145]
Ni_1Fe_9-CaO	Citric acid-based sol–gel with nitrate precursors	650 °C, 10% CO_2/N_2	650 °C, H_2	14.78	82.5	10 cycles, 20.9% loss	[143]
$Fe_5Co_5Mg_{10}$CaO	Citric acid-based sol–gel with nitrate precursors	650 °C, 10% CO_2/N_2	650 °C, H_2	9.2	90	10 cycles, stable	[142]

In a recent work by Wu et al., Ni-CaO-CeO_2 DFMs were synthesized via their acetate/nitrate precursors, using several methods including wet mixing, co-precipitation, and a citric acid-based sol–gel pathway [105]. Among the synthesized samples, DFMs prepared by sol–gel method exhibited superior physicochemical properties and hence displayed the highest CO_2 capture capacities and conversion, as well as CO yields and selectivity. In particular, the sol–gel-derived material with acetate precursors showed a CO_2 uptake of 15.34 mmol/g and CO_2 conversion of 92.4%, with CO selectivity of 89.1% at 650 °C. Meanwhile, the material prepared with nitrate precursors displayed a lower CO_2 uptake of 13.15%, but higher CO_2 conversion of 96% and higher CO selectivity (87–96%). It was concluded that, firstly, the sol–gel synthesis resulted in an optimal morphology and internal structure for the CO_2 capture and conversion. For instance, large BET surface areas and pore volumes facilitated CO_2 diffusion and adsorption, whereas an enhanced surface basicity promoted CO_2 affinity. Meanwhile, a smaller NiO grain size, uniform Ni dispersion, and higher reducibility could have led to improved catalytic activity. Secondly, the choice of acetate/nitrate precursors could affect catalyst–support interactions, which in turn result in variations in CO_2 uptake and conversion, CO selectivity, as well as the material's stability upon recycle.

Similar DFMs consisting of Ni over Ce-modified CaO were reported earlier by Sun et al., who employed a sol–gel method with citric acid [111]. The incorporation of CeO_2 was found to enhance the material's stability due to the formation of well-dispersed CeO_2 that can effectively prevent the growth and agglomeration of CaO and NiO crystallites, resulting in a stable performance after 20 cycles. This is reflected by the synthesized material with Ca/Ni/Ce molar ratio of 1:0.1:0.033, which exhibited a CO_2 uptake of 14.1 mmol/g, 51.8% CO_2 conversion, and almost 100% CO selectivity at 650 °C. The authors proposed possible reaction mechanisms which are based on a redox (Scheme 1) or associative formate (Scheme 2) mechanism, as illustrated in Figure 19. According to the redox mechanism, upon switching to the hydrogenation step, the adsorbed CO_2 could spill over to the Ni active sites, which may result in the formation of CO and NiO. In the presence of CeO_2, the oxygen vacancy on the CeO_2 surface may also interact with CO_2, leading to the formation of CO and the oxidation of Ce^{3+} species. The introduction of H_2 into the reactor would subsequently reduce NiO back to Ni and release H_2O molecules. Likewise, the adsorbed H_2 species on the CeO_2 surface extracts the lattice oxygen from ceria, releasing a H_2O molecule along with the reduction of the catalyst. Alternatively, the associative formate mechanism suggests that the adsorbed CO_2 on the CeO_2 surface may form bidentate formate as a reaction intermediate, which decomposes to form CO and terminal hydroxyl groups. Subsequently, the adsorbed H_2 reacts with the hydroxyl group, releasing a H_2O molecule.

In another study by Guo et al., ZrO_2 was used as a dopant for Ni/CaO, where it enhanced the surface basicity and reducibility of the DFM, resulting in an increased CO_2 uptake and catalytic activity [146]. At the optimum 12 wt% ZrO_2 loading, the material exhibited a high CO_2 uptake of 16.7 mmol/g with 63.2% CO_2 conversion and a 10.5 mmol/g CO yield at 650 °C. The formation of $CaZrO_3$ was also found to reduce the sintering of CaO and NiO crystals. The further incorporation of CeO_2 into Ni/CaO-ZrO_2 resulted in increased CO_2 conversion to 72.1% due to the increase of an oxygen vacancy, although the CO_2 uptake capacity decreased to 11.9 mmol/g, which could be attributed to a lower surface area. A similar strategy was also implemented by Sun et al. who incorporated Fe into a Ni/CaO DFM. An optimum CO yield of 11.3 mmol/g was obtained by using Ni_1Fe_9-CaO at 650 °C. It was observed that the formation of $Ca_2Fe_2O_5$ acted as an oxygen carrier that promoted CO production and helped improve the stability of the DFM by acting as a physical barrier that slowed down CaO sintering [143].

As alternatives to transition-metal-based materials, Sasayama et al. prepared DFMs that only contain alkali/alkaline earth metals (e.g., Na, K, and Ca) supported on γ-Al_2O_3 via the impregnation method [144]. They were then tested with 5 vol% and 400 ppm CO_2 in N_2 to investigate the production of syngas under model flue gas or direct air capture modes, respectively. Upon testing with 5 vol% CO_2 at 500 °C, Na/Al_2O_3 exhibited a 0.135 mmol/g

CO_2 uptake with 77% CO_2 conversion and 99.8% CO selectivity. On the other hand, with 400 ppm CO_2, its CO_2 uptake was about 0.09 mmol/g with 77.7% CO_2 conversion and 94.3% CO selectivity. The results therefore indicate the potential use of transition-metal-free DFMs for ICCC process, although further works are needed to improve the materials' performance and to study the reaction mechanism as well as to understand the catalytic active sites.

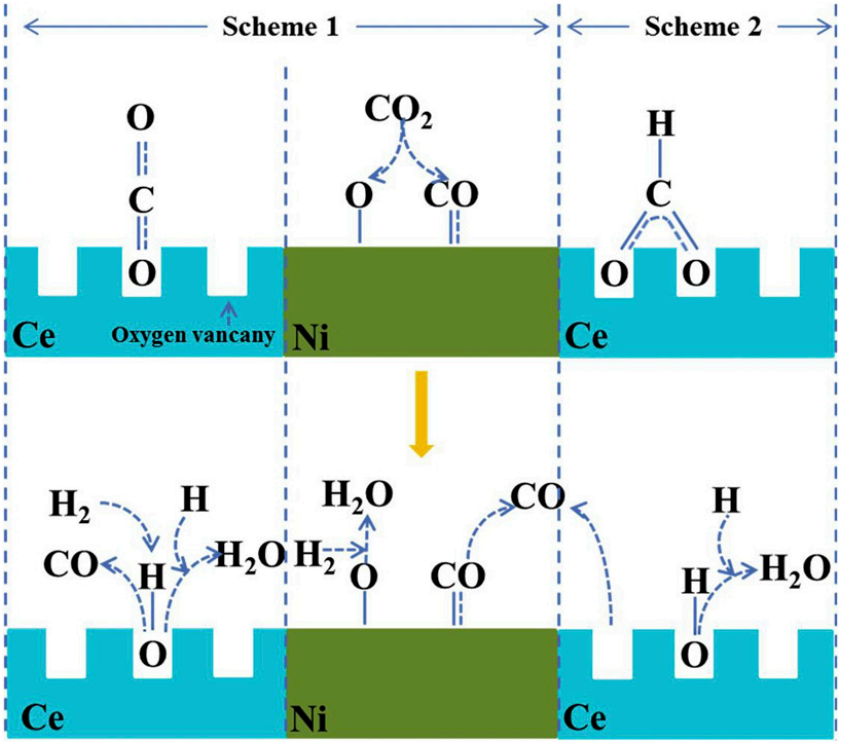

Figure 19. Reaction mechanism of RWGS over CeO_2-incorporated Ni/CaO DFM. Reprinted from ref. [111] with permission from the Elsevier.

In another study, the further incorporation of Pt on Na/Al_2O_3 was found to be selective for CO formation at lower temperatures of 350 °C [145], which is advantageous in reducing the typically high temperature requirement for the RWGS reaction. The DFM was prepared via the sequential impregnation method of Al_2O_3, first with Na, followed by Pt. The CO_2 capture was evaluated with 1% CO_2/10% O_2 in N_2, and its uptake capacity was found to be 0.19 mmol/g, comparable to that of Na/Al_2O_3 (0.21 mmol/g), and much higher than that of Pt/Al_2O_3 (0.08 mmol/g), indicating that Na serves as the CO_2 capture site. Upon hydrogenation, CO_2 was converted to CO with 89% conversion and 93% CO selectivity. In a control experiment, a physical mixture of Na/Al_2O_3 and Pt/Al_2O_3 was tested, and it was found that CO_2 conversion and CO selectivity decreased significantly to only 57% and 41%, respectively. The EDX spectroscopy (Figure 20) suggests that a core–shell structure of Pt-Na nanoparticles was formed on Pt-Na/Al_2O_3, with Pt as the core. As a result of the close interaction between the two metals, the Na species not only serves as the CO_2 capture site, but also as a promoter to enhance CO formation. Through in situ FTIR measurements, it was found that the adsorbed CO species was hardly observed over the material's surface, indicating that the presence of the Na species inhibited the adsorption of the generated CO, leading to high selectivity for CO.

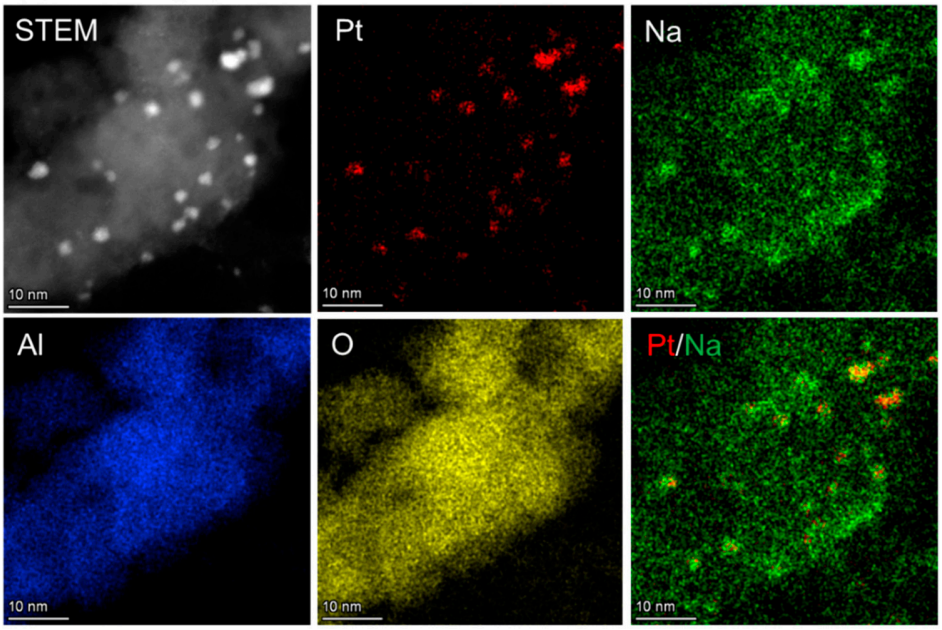

Figure 20. STEM image and EDX elemental mapping of Pt–Na/Al_2O_3. Reprinted from ref. [145] with permission from the American Chemical Society.

5.3. ICCC with Dry Reforming of Methane (DRM)

Besides RWGS, syngas can also be produced via the dry reforming of methane (DRM), where two potent greenhouse gases, CH_4 and CO_2, react with each other according to the following equation (Equation (17)):

$$CO_2 + CH_4 \rightarrow 2CO + 2H_2 \Delta H_R = 247.3 \frac{kJ}{mol} \quad (17)$$

Despite being favored for its "greening" capability, ICCC with DRM faces several disadvantages at industrial scales. First, the highly endothermic reaction requires a large energy input (Equation (17)). Second, the DFMs that catalyze the DRM reaction typically contain Ni in the catalytic component, which is susceptible to poisoning and deactivation via coking in the absence of steam. It has, therefore, been proposed that continued research in this field would focus on developing Ni-based DFMs that exhibit stronger coking resistance, e.g., by including alkaline promoters like Mg, or considering the use of Rh- or Ru-based DFMs to catalyze the reaction, in addition to uncovering further insights into the mechanisms of DRM so as to strengthen and optimize its industrial applicability [134,148]. The summary of DFMs that catalyze the DRM reaction is presented in Tables 5 and 6. The two tables categorize works according to their presentation of the ICCC performances of DFMs. In the former, the conversions of CO_2 and CH_4 are presented, whereas the yields of H_2 and CO are presented in the latter.

Table 5. Literature summary of DFMs that catalyze the dry reforming reaction (with conversions of CO_2 and CH_4).

DFM	Synthesis Method	Carbonation Conditions	Dry Reforming Conditions	CO_2 Sorption Capacity	CO_2 Conversion	CH_4 Conversion	Ref.
Ni_{10}-$(K\text{-}Mg)_{25}$/$(\gamma\text{-}Al_2O_3)_{75}$	Sol–gel/wet impregnation	650 °C, 10%CO_2/N_2	650 °C, 5%C_2H_6/N_2	0.22 mmol/g DFM	14%	16% (ethane)	[91]
Ni_{10}-$(Na\text{-}Mg)_{50}$/$(\gamma\text{-}Al_2O_3)_{50}$	Sol–gel/wet impregnation	650 °C, 10%CO_2/N_2	650 °C, 5%C_2H_6/N_2	0.16 mmol/g DFM	60%	47% (ethane)	[91]
Ni_{10}-$(K\text{-}Ca)_{50}$/$(\gamma\text{-}Al_2O_3)_{50}$	Sol–gel/wet impregnation	650 °C, 10%CO_2/N_2	650 °C, 5%C_2H_6/N_2	0.99 mmol/g DFM	65%	100% (ethane)	[91]
Ni_{10}-$(Na\text{-}Ca)_{50}$/$(\gamma\text{-}Al_2O_3)_{50}$	Sol–gel/wet impregnation	650 °C, 10%CO_2/N_2	650 °C, 5%C_2H_6/N_2	0.63 mmol/g DFM	75%	100% (ethane)	[91]
Ni/Ca-Zr	Precipitation/ammoniacal sol/impregnation	720 °C, 5%CO_2/Ar	720 °C, 8%CH_4/Ar	~3.64 mmol/g CaO (25 cycles)	-	~32%	[149]
NiCe/Ca-Zr	Precipitation/ammoniacal sol/impregnation	720 °C, 5%CO_2/Ar	720 °C, 8%CH_4/Ar	~5 mmol/g CaO (25 cycles)	-	~45%	[149]
Ni/MgO-Al_2O_3 (mixed with CaO)	Co-precipitation	720 °C, 20%CO_2/N_2	720 °C, 2.4%CH_4/N_2	14.1 mmol/g DFM (initial)	99.92%	99.94%	[150]
Ca-Fe-Mg oxide	Co-precipitation	600 °C, 100%CO_2	900 °C, 4.5%CH_4/N_2	0.64 mmol/g DFM	-	~50%	[151]

Table 6. Literature summary of DFMs that catalyze the dry reforming reaction (with yields of H_2 and CO).

DFM	Synthesis Method	Carbonation Conditions	Dry Reforming Conditions	CO_2 Sorption Capacity	H_2 Yield	CO Yield	Ref.
CaO/Ni_4	Sol–gel	600 °C, 20%CO_2/N_2	800 °C, 20%CH_4/N_2	~5.7 mmol/g CaO (initial)	5 mmol/g DFM	4.3 mmol/g DFM	[152]
CaO/Ni_9	Sol–gel	600 °C, 20%CO_2/N_2	800 °C, 20%CH_4/N_2	~5.1 mmol/g CaO (initial)	5 mmol/g DFM	4.5 mmol/g DFM	[152]
CaO/Ni_{19}	Sol–gel	600 °C, 20%CO_2/N_2	800 °C, 20%CH_4/N_2	~4.5 mmol/g CaO (initial)	3.5 mmol/g DFM	3.5 mmol/g DFM	[152]
Ni-CaO catal-sorbents	Sol–gel	700 °C, 10%CO_2/10%H_2O/N_2	700 °C, 10%CH_4/N_2	14.8 mmol/g DFM	131.7 mmol/g DFM	20.2 mmol/g DFM	[153]

Table 6. *Cont.*

DFM	Synthesis Method	Carbonation Conditions	Dry Reforming Conditions	CO_2 Sorption Capacity	H_2 Yield	CO Yield	Ref.
$Ni/Ca_{85}Ce_{15}$	Hydrothermal (sorbent); impregnation (DFM)	650 °C, 10%CO_2/Ar	650 °C, 6%CH_4/Ar	~13 mmol/g CaO (initial)	-	-	[154]
15% Ni-1% Ru, 10% $Na_2O/CeO_2–Al_2O_3$	Sequential impregnation	650 °C, 10%CO_2/N_2	650 °C, 10%CH_4/N_2	0.16 mmol/g DFM	25.774 mmol/g DFM	0.153 mmol/g DFM	[155]
15% Ni-1% Ru, 10% $K_2O/CeO_2–Al_2O_3$	Sequential impregnation	650 °C, 10%CO_2/N_2	650 °C, 10%CH_4/N_2	0.18 mmol/g DFM	22.512 mmol/g DFM	0.239 mmol/g DFM	[155]
15% Ni-1% Ru, 10% $CaO/CeO_2–Al_2O_3$	Sequential impregnation	650 °C, 10%CO_2/N_2	650 °C, 10%CH_4/N_2	0.26 mmol/g DFM	32.639 mmol/g DFM	0.338 mmol/g DFM	[155]
CaO-0.05Ni-0.05CeO_2	Co-precipitation	600 °C, 2%CO_2/N_2	800 °C, 2%CH_4/N_2	10.3 mmol/g CaO (initial); 7.9 mmol/g CaO (10th cycle)	754.4 mmol/g Ni (max, 2nd cycle)	454.6 mmol/g Ni (max, 2nd cycle)	[156]

In an earlier work, Kim et al. first demonstrated the calcium looping process combined with a catalytic system by using a physical mixture of CaO and Ni/MgO-Al_2O_3 as the CO_2 sorbent and DRM catalyst, respectively, in a single fluidized bed reactor [150]. The two-step process was operated in a cyclic manner where CO_2 was first captured on CaO during the carbonation step. Upon gas switching to CH_4, the CaO sorbent was regenerated while releasing CO_2, which instantaneously reacted with CH_4 on the Ni/MgO-Al_2O_3 catalyst, as depicted in Figure 21. CaO was derived from limestone via calcination at 800 °C whereas the Ni catalyst was derived from a hydrotalcite precursor that was synthesized via the co-precipitation method. At 720 °C, the CO_2 capture capacity was 14.1 mmol/g in the first cycle with an almost 100% conversion of CO_2 and CH_4. The resulting syngas thus had a H_2:CO ratio of 1.06:1. Due to the sintering of CaO, there was a significant loss of CO_2 uptake, which decreased to 9 mmol/g after 10 cycles of the reaction. Although, initially, Ni catalyst deactivation was observed due to coke formation, the carbon deposition amount was decreasing with increasing cycle numbers. It was found that the deposited carbon was removed during the carbonation step while the Ni metallic state was preserved, which could be due to the reverse Boudouard reaction $C + CO_2 \rightleftarrows 2CO$ that is favorable at high temperatures [152]. Therefore, CO_2 and CH_4 conversion can be maintained above 95% throughout the 10 cycles.

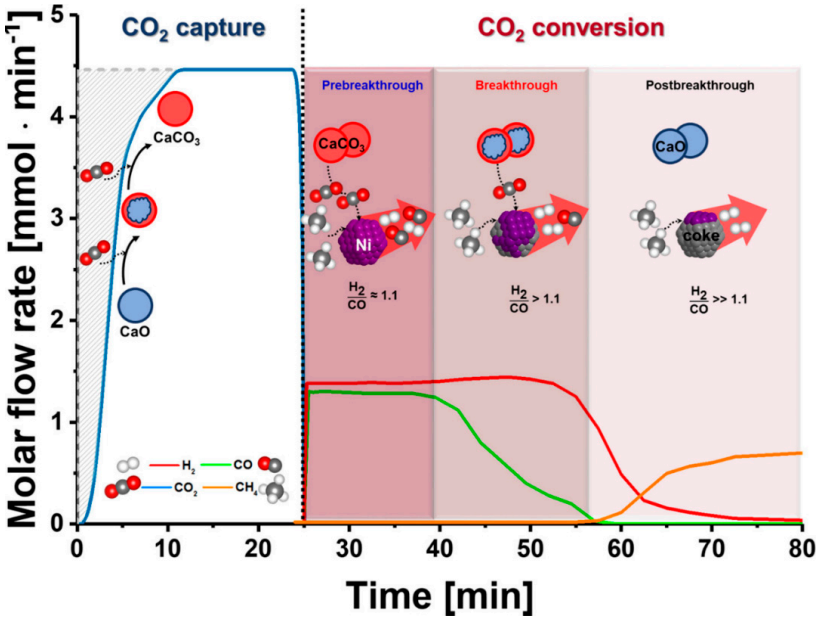

Figure 21. Cyclic process of ICCC with DRM over physical mixture of CaO and Ni/MgO-Al_2O_3 as CO_2 sorbent and catalyst, respectively. Reprinted from ref. [150] with permission from the American Chemical Society.

In subsequent works by Tian et al., a Ni/CaO-based DFM was prepared via citrate-based sol–gel synthesis which produced an average syngas yield of around 9 mmol/g throughout 10 cycles [152] of CO_2 capture (at 600 °C) and conversion with CH_4 (at 800 °C). The experimental H_2:CO ratio was about 1.1, higher than the theoretical ratio of 1. As the average CH4 conversion (86%) was higher than that of CO_2 (65%), it could be suggested that the Ni-CaO interface in the DFM was more active in dissociating CH_4 to yield H_2 than reducing CO_2 to yield CO. On the other hand, despite using a Ni/CaO DFM prepared with a similar method, Jo et al. obtained syngas with a high H_2:CO ratio of 6.52 at 700 °C, indicating that the CO_2 reduction reaction was suppressed [153]. It was observed that a large amount of carbon deposit was formed on the DFM, as well as the hydration of CaO to form $Ca(OH)_2$.

A further improvement of the Ni/CaO DFM was reported by Hu et al. where porous CeO_2-modified CaO microparticles were used as the support for Ni impregnation [154].

The introduction of CeO_2 into the material enhanced the DFM performance in two aspects, in that it acted as (i) a promoter that enhanced the CO_2 affinity towards CaO through the increase in lattice oxygen, thus enabling a high CO_2 uptake, and (ii) a physical stabilizer that enhanced the sintering resistance of CaO, improved Ni particle dispersion through the formation of small Ni crystallites, as well as increased Ni reducibility, thus enabling high and stable catalytic activity. Among the investigated samples, the material with 85%CaO:15%CeO_2 ($Ni/Ca_{85}Ce_{15}$) showed a constant CO_2 uptake and retained about 80–90% of its initial syngas time-averaged space time yield (STY) over nine cycles of CO_2 sorption and conversion at 650 °C, as shown in Figure 22. In another experiment, a layer of ZrO_2 was coated on $CaCO_3$ nanoparticles, followed by the co-impregnation of Ni and Ce [149]. During the CO_2 capture–DRM cycle tests at 720 °C, 5% CO_2 was used as the gas feed to mimic flue gas composition where over 40% conversion of CO_2 and CH_4 can be achieved. The presence of ZrO_2 was also found to enhance material stability by preventing sintering. Through the in situ DRIFTS analysis (Figure 23), monodentate carbonate was observed on the CaO surface during the carbonation step, whereas polydentate carbonate was observed on ZrO_2 and bidentate carbonate on the CeO_2 surface. CO_2 dissociation to CO was also detected on NiCe/Ca-Zr oxide due to the presence of abundant oxygen vacancies on the reduced CeO_2. Upon gas switching to CH_4, the characteristic IR peaks of formate species and gaseous CO were observed, while carbonate peak intensities were decreased. These suggested that the occurrence of $CaCO_3$ decarbonation was coupled with the DRM reaction, during which the adsorbed H species produced from CH_4 decomposition reacted with the CO_3^{2-} species to form formate species, which further decomposed to CO [149].

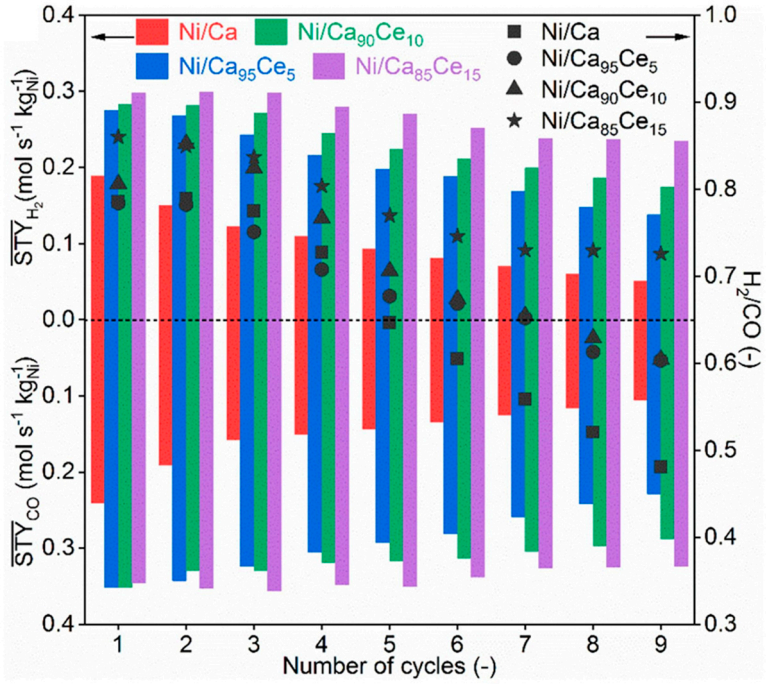

Figure 22. Time-averaged space time yield (STY) of H_2 (top) and CO (bottom) of the prepared Ni/CeO_2-CaO DFMs with various CaO:CeO_2 molar ratio throughout 9 cycles of CO_2 capture and conversion at 650 °C. Ni/CaO was used as reference material. Reprinted from ref. [154] with permission from Elsevier.

The combination of Ni with Ru supported on CeO_2/Al_2O_3 containing Na_2O, K_2O, or CaO was reported by Merkouri et al. [155]. The DFMs contained 15%Ni and 1%Ru, and were mostly active for ICCC with DRM at 650 °C, where the CaO-containing material produced 0.338 mmol/g CO and 32.6 mmol/g H_2, yielding H_2-rich syngas. The large formation of H_2 during DRM was mainly due to methane cracking and its decomposition into carbon, evidenced by CH_4-TPSR experiments which showed that methane cracking

peaked at around 635 °C. By using an operando DRIFTS-MS method, the authors elucidated the CO_2 capture and reaction mechanism over the Ni-Ru-Na_2O/CeO_2-Al_2O_3 DFM through alternating successive CO_2 and CH_4 cycles at 550 °C. In agreement with Tian et al.'s previous work [152], CH_4 reduction on the metallic sites produced a H_2 and graphitic carbon layer, which further gasified with CO_2 during the capture step to yield CO through a reverse Bourdouard reaction. However, it was noted that the coke gasification kinetics were slower than the coke formation, resulting in the rapid deactivation of the catalyst. This mechanistic study thus highlights the importance of controlling CH_4 cracking during the DRM reaction via optimizing the material's design and reaction engineering in order to slow down the catalyst deactivation, as well as to obtain syngas with a favorable H_2:CO ratio.

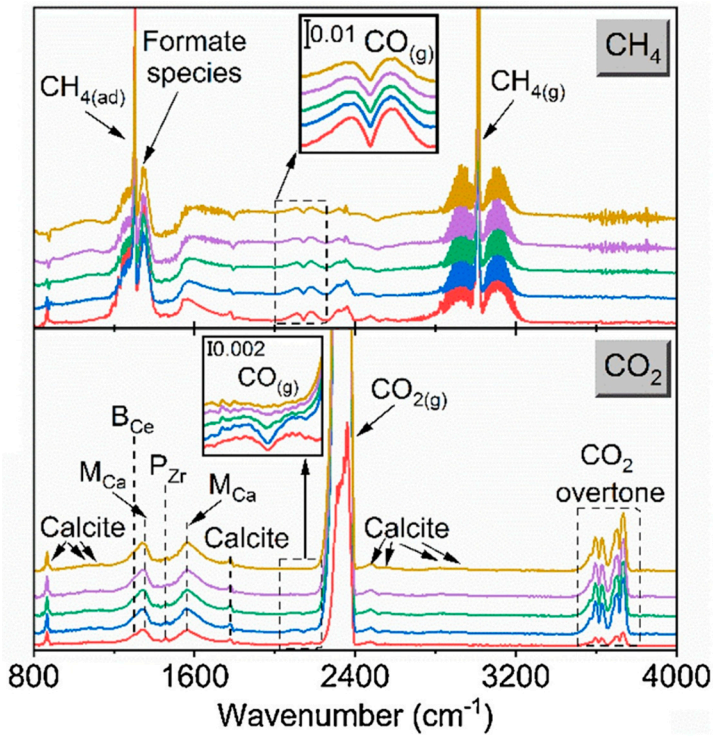

Figure 23. In situ DRIFTS spectra of the reduced NiCe/Ca@Zr in CO_2 and CH_4 environment at 550 °C and 1 bar, with different color to represent spectrum obtained at different time during exposure in different gas environment. Abbreviation—(g): gas phase; (ad): adsorbed; MCa: Monodentate carbonate on CaO surface; PZr: Polydentate carbonate on ZrO_2 surface; BCe: Bidentate carbonate on CeO_2 surface. Reprinted from ref. [149] with permission from Elsevier.

Further alternatives that include the dry reforming of other hydrocarbons, such as ethane (DRE), to produce syngas (Equation (18)) was reported by Al-Mamoori et al. [91], who investigated the use of CaO- and MgO-based double salts promoted by K/Ca, supported on alumina, and impregnated with Ni as the catalyst at 650 °C.

$$CO_2 + C_2H_6 \rightarrow 4CO + 3H_2; \Delta H_R = 428.1 \frac{kJ}{mol} \quad (18)$$

The material's synthetic methods consisted of a sol–gel method for the alumina support, while the adsorbent and catalyst components were incorporated via wet impregnation. The CaO-based DFMs comprising 20 wt% Ni and a 1:1 ratio of adsorbent to support showed the best ICCC performance, with CO_2 adsorption capacities of 0.99 mmol/g and 0.63 mmol/g for the K-Ca-based and Na-Ca-based DFMs, respectively, a 65% and 75% conversion of CO_2 for the K-Ca-based and Na-Ca-based DFMs, respectively, and a 100% C_2H_6 conversion for both DFMs. Additionally, yields of approximately 45% and 37.5% for CO and H_2, respectively, were reported for the K-Ca-based DFM when subjected to a

sustained DRE process (up to 10 h) at 650 °C. Despite a relatively stable performance, coke formation (9 wt%) was observed due to a high Ni content. From their investigations, it was concluded that the adsorbent/catalyst contents directly influenced CO_2 capture and conversion performances, and that reaction conditions strongly influenced the selectivity toward DRE or the occurrence of side reactions, such as oxidative dehydrogenation, ethane cracking, RWGS, and coking. Therefore, it is imperative to optimize their chemical and physical properties.

6. Perspectives and Future Outlook

It is evident that DFMs have increasingly played an important role in decarbonization efforts through CO_2 recycling and reutilization. Through numerous studies in the past decade, DFMs have shown to offer feasibility and versatility in capturing CO_2 from both model flue gas and air (direct air capture), and subsequently converting it to other C1 species, such as methane and syngas. The recent literature has reported extensive DFM formulations and configurations for ICCC that primarily include Ni, Ru, and Rh as the catalytic metals, basic oxides such as Na_2O, K_2O, CaO, and MgO as the CO_2 sorbents, and Al_2O_3 as a common support. From the various given examples, the combinations of these materials are shown to form flexible DFMs that catalyze CO_2 methanation, RWGS, and DRM, each of which has its own optimum operating conditions. For example, CO_2 methanation is favored at an intermediate temperature range of 300–350 °C, whereas RWGS and DRM are favored at high temperatures (600–750 °C).

The effectiveness of DFMs is determined by both their CO_2 capture capacity and catalytic activity. The CO_2 uptake principally depends on (i) the basicity of the materials, with medium to strong basic sites favorable for CO_2 adsorption, and (ii) the surface area and porosity. On the other hand, the catalytic activity depends on several factors, such as (i) the crystallite size and dispersion of the active metals, with a small size and high metal dispersion attributed to high catalytic activity, (ii) the reducibility of the active metals, which is determined by the interaction between the active metal particles and the oxide support, (iii) the basicity of the material, where weak basic sites are beneficial for CO_2 methanation and medium basic sites for the RWGS and DRM [155], and (iv) the availability of oxygen vacancies, which can often be enhanced by incorporating a dopant, such as CeO_2. In fact, there is a recent review by Hussain et al. that discusses the importance of oxygen vacancies for CO_2 methanation and its tuning strategies [157].

Given the complexity in developing and tuning DFMs with the desired properties, major progress has been achieved at the laboratory scale, leading to several promising candidates with good CO_2 conversion and product selectivity. However, there are still many challenges to implement ICCC with DFMs on a larger scale. For instance, the stability and recyclability of the materials need to be improved as DFMs are susceptible to sintering, coking, and poisoning. It, therefore, requires careful material engineering to synthesize robust DFMs that can withstand harsh conditions upon prolonged and repeated cycles. In view of this, lifetime studies of DFMs need to be carried out under real flue gas conditions that typically contain moisture, O_2, and other impurities, such as NO_x, to guarantee their industrial viability. To accelerate the screening process, the use of computational DFT modeling would be highly encouraged to aid in the fine-tuning of the material's properties while studying the reaction mechanisms to control the desired product selectivity as well as to minimize catalyst deactivation.

Considering that ICCC with DFMs is an emerging field, there are plenty of research opportunities in the future to develop versatile and robust DFMs that enable the production of other chemicals, such as alcohols and longer-chain hydrocarbons, which could offer the greater flexibility of producing different products within the same production facility. We believe that the advancement of this technology will continue promoting sustainable chemical manufacturing and a low carbon economy.

Author Contributions: Conceptualization, W.J.T. and P.G.; Methodology, W.J.T. and P.G.; Writing—original draft preparation, W.J.T. and P.G.; Writing—review and editing, W.J.T. and P.G.; Project administration, P.G.; Funding acquisition, P.G. All authors have read and agreed to the published version of the manuscript.

Funding: This research was funded by the C. N. Yang Scholars Program at Nanyang Technological University AY2022-2023.

Acknowledgments: This research was made possible by the C. N. Yang Scholars Program at Nanyang Technological University.

Conflicts of Interest: The authors declare no conflict of interest.

References

1. *An IPCC Special Report on the Impacts of Global Warming of 1.5 °C above Pre-Industrial Levels and Related Global Greenhouse Gas Emission Pathways, in the Context of Strengthening the Global Response to the Threat of Climate Change, Sustainable Development, and Efforts to Eradicate Poverty*; Intergovernmental Panel on Climate Change: Geneva, Switzerland, 2018.
2. Koytsoumpa, E.I.; Bergins, C.; Kakaras, E. The CO_2 economy: Review of CO_2 capture and reuse technologies. *J. Supercrit. Fluids* **2018**, *132*, 3–16. [CrossRef]
3. Leeson, D.; Mac Dowell, N.; Shah, N.; Petit, C.; Fennell, P.S. A Techno-economic analysis and systematic review of carbon capture and storage (CCS) applied to the iron and steel, cement, oil refining and pulp and paper industries, as well as other high purity sources. *Int. J. Greenh. Gas Control* **2017**, *61*, 71–84. [CrossRef]
4. Naims, H. Economics of carbon dioxide capture and utilization—A supply and demand perspective. *Environ. Sci. Pollut. Res.* **2016**, *23*, 22226–22241. [CrossRef] [PubMed]
5. Wilberforce, T.; Baroutaji, A.; Soudan, B.; Al-Alami, A.H.; Olabi, A.G. Outlook of carbon capture technology and challenges. *Sci. Total Environ.* **2019**, *657*, 56–72. [CrossRef]
6. Omodolor, I.S.; Otor, H.O.; Andonegui, J.A.; Allen, B.J.; Alba-Rubio, A.C. Dual-Function Materials for CO_2 Capture and Conversion: A Review. *Ind. Eng. Chem. Res.* **2020**, *59*, 17612–17631. [CrossRef]
7. von der Assen, N.; Bardow, A. Life cycle assessment of polyols for polyurethane production using CO_2 as feedstock: Insights from an industrial case study. *Green Chem.* **2014**, *16*, 3272–3280. [CrossRef]
8. Artz, J.; Müller, T.E.; Thenert, K.; Kleinekorte, J.; Meys, R.; Sternberg, A.; Bardow, A.; Leitner, W. Sustainable Conversion of Carbon Dioxide: An Integrated Review of Catalysis and Life Cycle Assessment. *Chem. Rev.* **2018**, *118*, 434–504. [CrossRef]
9. Huang, C.-H.; Tan, C.-S. A Review: CO_2 Utilization. *Aerosol Air Qual. Res.* **2014**, *14*, 480–499. [CrossRef]
10. Freyman, M.C.; Huang, Z.; Ravikumar, D.; Duoss, E.B.; Li, Y.; Baker, S.E.; Pang, S.H.; Schaidle, J.A. Reactive CO_2 capture: A path forward for process integration in carbon management. *Joule* **2023**, *7*, 631–651. [CrossRef]
11. Duyar, M.S.; Treviño, M.A.A.; Farrauto, R.J. Dual function materials for CO_2 capture and conversion using renewable H_2. *Appl. Catal. B Environ.* **2015**, *168–169*, 370–376. [CrossRef]
12. Melo Bravo, P.; Debecker, D.P. Combining CO_2 capture and catalytic conversion to methane. *Waste Dispos. Sustain. Energy* **2019**, *1*, 53–65. [CrossRef]
13. Merkouri, L.-P.; Reina, T.R.; Duyar, M.S. Closing the Carbon Cycle with Dual Function Materials. *Energy Fuels* **2021**, *35*, 19859–19880. [CrossRef]
14. Sun, S.; Sun, H.; Williams, P.T.; Wu, C. Recent advances in integrated CO_2 capture and utilization: A review. *Sustain. Energy Fuels* **2021**, *5*, 4546–4559. [CrossRef]
15. Sabri, M.A.; Al Jitan, S.; Bahamon, D.; Vega, L.F.; Palmisano, G. Current and future perspectives on catalytic-based integrated carbon capture and utilization. *Sci. Total Environ.* **2021**, *790*, 148081. [CrossRef] [PubMed]
16. Li, H.; Dang, C.; Yang, G.; Cao, Y.; Wang, H.; Peng, F.; Yu, H. Bi-functional particles for integrated thermo-chemical processes: Catalysis and beyond. *Particuology* **2021**, *56*, 10–32. [CrossRef]
17. Bhatta, L.K.G.; Subramanyam, S.; Chengala, M.D.; Olivera, S.; Venkatesh, K. Progress in hydrotalcite like compounds and metal-based oxides for CO_2 capture: A review. *J. Clean. Prod.* **2015**, *103*, 171–196. [CrossRef]
18. Khalilpour, R.; Mumford, K.; Zhai, H.; Abbas, A.; Stevens, G.; Rubin, E.S. Membrane-based carbon capture from flue gas: A review. *J. Clean. Prod.* **2015**, *103*, 286–300. [CrossRef]
19. Al-Mamoori, A.; Krishnamurthy, A.; Rownaghi, A.A.; Rezaei, F. Carbon Capture and Utilization Update. *Energy Technol.* **2017**, *5*, 834–849. [CrossRef]
20. Yang, Z.-Z.; Wei, J.-J.; Zeng, G.-M.; Zhang, H.-Q.; Tan, X.-F.; Ma, C.; Li, X.-C.; Li, Z.-H.; Zhang, C. A review on strategies to LDH-based materials to improve adsorption capacity and photoreduction efficiency for CO_2. *Coord. Chem. Rev.* **2019**, *386*, 154–182. [CrossRef]
21. Xie, K.; Fu, Q.; Qiao, G.G.; Webley, P.A. Recent progress on fabrication methods of polymeric thin film gas separation membranes for CO_2 capture. *J. Membr. Sci.* **2019**, *572*, 38–60. [CrossRef]
22. Gao, W.; Liang, S.; Wang, R.; Jiang, Q.; Zhang, Y.; Zheng, Q.; Xie, B.; Toe, C.Y.; Zhu, X.; Wang, J.; et al. Industrial carbon dioxide capture and utilization: State of the art and future challenges. *Chem. Soc. Rev.* **2020**, *49*, 8584–8686. [CrossRef] [PubMed]

23. Younas, M.; Rezakazemi, M.; Daud, M.; Wazir, M.B.; Ahmad, S.; Ullah, N.; Inamuddin; Ramakrishna, S. Recent progress and remaining challenges in post-combustion CO_2 capture using metal-organic frameworks (MOFs). *Prog. Energy Combust. Sci.* **2020**, *80*, 100849. [CrossRef]
24. Zheng, J.; Chong, Z.R.; Qureshi, M.F.; Linga, P. Carbon Dioxide Sequestration via Gas Hydrates: A Potential Pathway toward Decarbonization. *Energy Fuels* **2020**, *34*, 10529–10546. [CrossRef]
25. Dunstan, M.T.; Donat, F.; Bork, A.H.; Grey, C.P.; Müller, C.R. CO_2 Capture at Medium to High Temperature Using Solid Oxide-Based Sorbents: Fundamental Aspects, Mechanistic Insights, and Recent Advances. *Chem. Rev.* **2021**, *121*, 12681–12745. [CrossRef] [PubMed]
26. Fu, L.; Ren, Z.; Si, W.; Ma, Q.; Huang, W.; Liao, K.; Huang, Z.; Wang, Y.; Li, J.; Xu, P. Research progress on CO_2 capture and utilization technology. *J. CO_2 Util.* **2022**, *66*, 102260. [CrossRef]
27. Dubey, A.; Arora, A. Advancements in carbon capture technologies: A review. *J. Clean. Prod.* **2022**, *373*, 133932. [CrossRef]
28. Peres, C.B.; Resende, P.M.R.; Nunes, L.J.R.; Morais, L.C.d. Advances in Carbon Capture and Use (CCU) Technologies: A Comprehensive Review and CO_2 Mitigation Potential Analysis. *Clean Technol.* **2022**, *4*, 1193–1207. [CrossRef]
29. Idem, R.; Supap, T.; Shi, H.; Gelowitz, D.; Ball, M.; Campbell, C.; Tontiwachwuthikul, P. Practical experience in post-combustion CO_2 capture using reactive solvents in large pilot and demonstration plants. *Int. J. Greenh. Gas Control* **2015**, *40*, 6–25. [CrossRef]
30. Li, Y.; Li, L.; Yu, J. Applications of Zeolites in Sustainable Chemistry. *Chem* **2017**, *3*, 928–949. [CrossRef]
31. Suescum-Morales, D.; Jiménez, J.R.; Fernández-Rodríguez, J.M. Review of the Application of Hydrotalcite as CO_2 Sinks for Climate Change Mitigation. *ChemEngineering* **2022**, *6*, 50. [CrossRef]
32. Veerabhadrappa, M.G.; Maroto-Valer, M.M.; Chen, Y.; Garcia, S. Layered Double Hydroxides-Based Mixed Metal Oxides: Development of Novel Structured Sorbents for CO_2 Capture Applications. *ACS Appl. Mater. Interfaces* **2021**, *13*, 11805–11813. [CrossRef] [PubMed]
33. Gao, W.; Zhou, T.; Gao, Y.; Louis, B.; O'Hare, D.; Wang, Q. Molten salts-modified MgO-based adsorbents for intermediate-temperature CO_2 capture: A review. *J. Energy Chem.* **2017**, *26*, 830–838. [CrossRef]
34. Kwak, J.-S.; Kim, K.-Y.; Oh, K.-R.; Kwon, Y.-U. Performance enhancement of all-solid CO_2 absorbent based on Na_2CO_3-promoted MgO by using ZrO_2 dispersant. *Int. J. Greenh. Gas Control* **2019**, *81*, 38–43. [CrossRef]
35. Joo, H.; Cho, S.J.; Na, K. Control of CO_2 absorption capacity and kinetics by MgO-based dry sorbents promoted with carbonate and nitrate salts. *J. CO_2 Util.* **2017**, *19*, 194–201. [CrossRef]
36. Jeon, H.; Triviño, M.L.T.; Hwang, S.; Moon, J.H.; Yoo, J.; Seo, J.G. Unveiling the carbonation mechanism in molten salt-promoted MgO-Al_2O_3 sorbents. *J. CO_2 Util.* **2020**, *39*, 101153. [CrossRef]
37. Hu, Z.; Wang, Y.; Shah, B.B.; Zhao, D. CO_2 Capture in Metal–Organic Framework Adsorbents: An Engineering Perspective. *Adv. Sustain. Syst.* **2019**, *3*, 1800080. [CrossRef]
38. Song, K.S.; Fritz, P.W.; Coskun, A. Porous organic polymers for CO_2 capture, separation and conversion. *Chem. Soc. Rev.* **2022**, *51*, 9831–9852. [CrossRef]
39. Wang, J.; Wang, L.; Wang, Y.; Zhang, D.; Xiao, Q.; Huang, J.; Liu, Y.-N. Recent progress in porous organic polymers and their application for CO_2 capture. *Chin. J. Chem. Eng.* **2022**, *42*, 91–103. [CrossRef]
40. Luo, R.; Chen, M.; Liu, X.; Xu, W.; Li, J.; Liu, B.; Fang, Y. Recent advances in CO_2 capture and simultaneous conversion into cyclic carbonates over porous organic polymers having accessible metal sites. *J. Mater. Chem. A* **2020**, *8*, 18408–18424. [CrossRef]
41. Silva, J.M.; Trujillano, R.; Rives, V.; Soria, M.A.; Madeira, L.M. High temperature CO_2 sorption over modified hydrotalcites. *Chem. Eng. J.* **2017**, *325*, 25–34. [CrossRef]
42. Miguel, C.V.; Trujillano, R.; Rives, V.; Vicente, M.A.; Ferreira, A.F.P.; Rodrigues, A.E.; Mendes, A.; Madeira, L.M. High temperature CO_2 sorption with gallium-substituted and promoted hydrotalcites. *Sep. Purif. Technol.* **2014**, *127*, 202–211. [CrossRef]
43. Faria, A.C.; Trujillano, R.; Rives, V.; Miguel, C.V.; Rodrigues, A.E.; Madeira, L.M. Alkali metal (Na, Cs and K) promoted hydrotalcites for high temperature CO_2 capture from flue gas in cyclic adsorption processes. *Chem. Eng. J.* **2022**, *427*, 131502. [CrossRef]
44. Lee, J.M.; Min, Y.J.; Lee, K.B.; Jeon, S.G.; Na, J.G.; Ryu, H.J. Enhancement of CO_2 Sorption Uptake on Hydrotalcite by Impregnation with K_2CO_3. *Langmuir* **2010**, *26*, 18788–18797. [CrossRef]
45. Halabi, M.H.; de Croon, M.H.J.M.; van der Schaaf, J.; Cobden, P.D.; Schouten, J.C. High capacity potassium-promoted hydrotalcite for CO_2 capture in H_2 production. *Int. J. Hydrogen Energy* **2012**, *37*, 4516–4525. [CrossRef]
46. Kim, S.; Lee, K.B. Impregnation of hydrotalcite with $NaNO_3$ for enhanced high-temperature CO_2 sorption uptake. *Chem. Eng. J.* **2019**, *356*, 964–972. [CrossRef]
47. Oliveira, E.L.G.; Grande, C.A.; Rodrigues, A.E. CO_2 sorption on hydrotalcite and alkali-modified (K and Cs) hydrotalcites at high temperatures. *Sep. Purif. Technol.* **2008**, *62*, 137–147. [CrossRef]
48. Perejón, A.; Romeo, L.M.; Lara, Y.; Lisbona, P.; Martínez, A.; Valverde, J.M. The Calcium-Looping technology for CO_2 capture: On the important roles of energy integration and sorbent behavior. *Appl. Energy* **2016**, *162*, 787–807. [CrossRef]
49. Benhelal, E.; Shamsaei, E.; Rashid, M.I. Challenges against CO_2 abatement strategies in cement industry: A review. *J. Environ. Sci.* **2021**, *104*, 84–101. [CrossRef]
50. Plaza, M.G.; Martínez, S.; Rubiera, F. CO_2 Capture, Use, and Storage in the Cement Industry: State of the Art and Expectations. *Energies* **2020**, *13*, 5692. [CrossRef]

51. MacKenzie, A.; Granatstein, D.L.; Anthony, E.J.; Abanades, J.C. Economics of CO_2 Capture Using the Calcium Cycle with a Pressurized Fluidized Bed Combustor. *Energy Fuels* **2007**, *21*, 920–926. [CrossRef]
52. Geng, Y.-q.; Guo, Y.-x.; Fan, B.; Cheng, F.-q.; Cheng, H.-g. Research progress of calcium-based adsorbents for CO_2 capture and anti-sintering modification. *J. Fuel Chem. Technol.* **2021**, *49*, 998–1013. [CrossRef]
53. Hu, Y.; Lu, H.; Liu, W.; Yang, Y.; Li, H. Incorporation of CaO into inert supports for enhanced CO_2 capture: A review. *Chem. Eng. J.* **2020**, *396*, 125253. [CrossRef]
54. Krödel, M.; Landuyt, A.; Abdala, P.M.; Müller, C.R. Mechanistic Understanding of CaO-Based Sorbents for High-Temperature CO_2 Capture: Advanced Characterization and Prospects. *ChemSusChem* **2020**, *13*, 6259–6272. [CrossRef] [PubMed]
55. Sun, H.; Wu, C.; Shen, B.; Zhang, X.; Zhang, Y.; Huang, J. Progress in the development and application of CaO-based adsorbents for CO_2 capture—A review. *Mater. Today Sustain.* 2018; 1–2, 1–27. [CrossRef]
56. Lu, H.; Khan, A.; Pratsinis, S.E.; Smirniotis, P.G. Flame-Made Durable Doped-CaO Nanosorbents for CO_2 Capture. *Energy Fuels* **2009**, *23*, 1093–1100. [CrossRef]
57. Li, L.; King, D.L.; Nie, Z.; Howard, C. Magnesia-Stabilized Calcium Oxide Absorbents with Improved Durability for High Temperature CO_2 Capture. *Ind. Eng. Chem. Res.* **2009**, *48*, 10604–10613. [CrossRef]
58. Lysikov, A.I.; Salanov, A.N.; Okunev, A.G. Change of CO_2 Carrying Capacity of CaO in Isothermal Recarbonation—Decomposition Cycles. *Ind. Eng. Chem. Res.* **2007**, *46*, 4633–4638. [CrossRef]
59. Grasa, G.S.; Abanades, J.C. CO_2 Capture Capacity of CaO in Long Series of Carbonation/Calcination Cycles. *Ind. Eng. Chem. Res.* **2006**, *45*, 8846–8851. [CrossRef]
60. Kierzkowska, A.M.; Pacciani, R.; Müller, C.R. CaO-Based CO_2 Sorbents: From Fundamentals to the Development of New, Highly Effective Materials. *ChemSusChem* **2013**, *6*, 1130–1148. [CrossRef]
61. Jing, J.-Y.; Li, T.-Y.; Zhang, X.-W.; Wang, S.-D.; Feng, J.; Turmel, W.A.; Li, W.-Y. Enhanced CO_2 sorption performance of $CaO/Ca_3Al_2O_6$ sorbents and its sintering-resistance mechanism. *Appl. Energy* **2017**, *199*, 225–233. [CrossRef]
62. Zhou, Z.; Qi, Y.; Xie, M.; Cheng, Z.; Yuan, W. Synthesis of CaO-based sorbents through incorporation of alumina/aluminate and their CO_2 capture performance. *Chem. Eng. Sci.* **2012**, *74*, 172–180. [CrossRef]
63. Han, R.; Gao, J.; Wei, S.; Su, Y.; Qin, Y. Development of highly effective $CaO@Al_2O_3$ with hierarchical architecture CO_2 sorbents via a scalable limited-space chemical vapor deposition technique. *J. Mater. Chem. A* **2018**, *6*, 3462–3470. [CrossRef]
64. Wang, N.; Feng, Y.; Liu, L.; Guo, X. Effects of preparation methods on the structure and property of Al-stabilized CaO-based sorbents for CO_2 capture. *Fuel Process. Technol.* **2018**, *173*, 276–284. [CrossRef]
65. López, J.M.; Grasa, G.; Murillo, R. Evaluation of the effect of inert support on the carbonation reaction of synthetic CaO-based CO_2 sorbents. *Chem. Eng. J.* **2018**, *350*, 559–572. [CrossRef]
66. Yu, Y.S.; Liu, W.Q.; An, H.; Yang, F.S.; Wang, G.X.; Feng, B.; Zhang, Z.X.; Rudolph, V. Modeling of the carbonation behavior of a calcium based sorbent for CO_2 capture. *Int. J. Greenh. Gas Control* **2012**, *10*, 510–519. [CrossRef]
67. Kurlov, A.; Broda, M.; Hosseini, D.; Mitchell, S.J.; Pérez-Ramírez, J.; Müller, C.R. Mechanochemically Activated, Calcium Oxide-Based, Magnesium Oxide-Stabilized Carbon Dioxide Sorbents. *ChemSusChem* **2016**, *9*, 2380–2390. [CrossRef] [PubMed]
68. Zhang, X.; Li, Z.; Peng, Y.; Su, W.; Sun, X.; Li, J. Investigation on a novel $CaO–Y_2O_3$ sorbent for efficient CO_2 mitigation. *Chem. Eng. J.* **2014**, *243*, 297–304. [CrossRef]
69. Naeem, M.A.; Armutlulu, A.; Imtiaz, Q.; Müller, C.R. CaO-Based CO_2 Sorbents Effectively Stabilized by Metal Oxides. *ChemPhysChem* **2017**, *18*, 3280–3285. [CrossRef]
70. Kim, S.M.; Kierzkowska, A.M.; Broda, M.; Müller, C.R. Sol-gel synthesis of $MgAl_2O_4$-stabilized CaO for CO_2 capture. *Energy Procedia* **2017**, *114*, 220–229. [CrossRef]
71. Koirala, R.; Reddy, G.K.; Smirniotis, P.G. Single nozzle flame-made highly durable metal doped Ca-based sorbents for CO_2 capture at high temperature. *Energy Fuels* **2012**, *26*, 3103–3109. [CrossRef]
72. Lu, H.; Smirniotis, P.G. Calcium oxide doped sorbents for CO_2 uptake in the presence of SO_2 at high temperatures. *Ind. Eng. Chem. Res.* **2009**, *48*, 5454–5459. [CrossRef]
73. De, S.; Dokania, A.; Ramirez, A.; Gascon, J. Advances in the Design of Heterogeneous Catalysts and Thermocatalytic Processes for CO_2 Utilization. *ACS Catal.* **2020**, *10*, 14147–14185. [CrossRef]
74. Younas, M.; Loong Kong, L.; Bashir, M.J.K.; Nadeem, H.; Shehzad, A.; Sethupathi, S. Recent Advancements, Fundamental Challenges, and Opportunities in Catalytic Methanation of CO_2. *Energy Fuels* **2016**, *30*, 8815–8831. [CrossRef]
75. Aziz, M.A.A.; Jalil, A.A.; Triwahyono, S.; Ahmad, A. CO_2 methanation over heterogeneous catalysts: Recent progress and future prospects. *Green Chem.* **2015**, *17*, 2647–2663. [CrossRef]
76. Fan, W.K.; Tahir, M. Recent trends in developments of active metals and heterogenous materials for catalytic CO_2 hydrogenation to renewable methane: A review. *J. Environ. Chem. Eng.* **2021**, *9*, 105460. [CrossRef]
77. Chen, X.; Chen, Y.; Song, C.; Ji, P.; Wang, N.; Wang, W.; Cui, L. Recent Advances in Supported Metal Catalysts and Oxide Catalysts for the Reverse Water-Gas Shift Reaction. *Front. Chem.* **2020**, *8*, 709. [CrossRef]
78. Daza, Y.A.; Kuhn, J.N. CO_2 conversion by reverse water gas shift catalysis: Comparison of catalysts, mechanisms and their consequences for CO_2 conversion to liquid fuels. *RSC Adv.* **2016**, *6*, 49675–49691. [CrossRef]
79. Nielsen, D.U.; Hu, X.-M.; Daasbjerg, K.; Skrydstrup, T. Chemically and electrochemically catalysed conversion of CO_2 to CO with follow-up utilization to value-added chemicals. *Nat. Catal.* **2018**, *1*, 244–254. [CrossRef]

80. le Saché, E.; Reina, T.R. Analysis of Dry Reforming as direct route for gas phase CO_2 conversion. The past, the present and future of catalytic DRM technologies. *Prog. Energy Combust. Sci.* **2022**, *89*, 100970. [CrossRef]
81. Jang, W.-J.; Shim, J.-O.; Kim, H.-M.; Yoo, S.-Y.; Roh, H.-S. A review on dry reforming of methane in aspect of catalytic properties. *Catal. Today* **2019**, *324*, 15–26. [CrossRef]
82. Singh, R.; Dhir, A.; Mohapatra, S.K.; Mahla, S.K. Dry reforming of methane using various catalysts in the process: Review. *Biomass Convers. Biorefinery* **2020**, *10*, 567–587. [CrossRef]
83. Dieterich, V.; Buttler, A.; Hanel, A.; Spliethoff, H.; Fendt, S. Power-to-liquid via synthesis of methanol, DME or Fischer–Tropsch-fuels: A review. *Energy Environ. Sci.* **2020**, *13*, 3207–3252. [CrossRef]
84. Atsbha, T.A.; Yoon, T.; Seongho, P.; Lee, C.-J. A review on the catalytic conversion of CO_2 using H_2 for synthesis of CO, methanol, and hydrocarbons. *J. CO_2 Util.* **2021**, *44*, 101413. [CrossRef]
85. Yang, H.; Zhang, C.; Gao, P.; Wang, H.; Li, X.; Zhong, L.; Wei, W.; Sun, Y. A review of the catalytic hydrogenation of carbon dioxide into value-added hydrocarbons. *Catal. Sci. Technol.* **2017**, *7*, 4580–4598. [CrossRef]
86. Tang, R.; Zhu, Z.; Li, C.; Xiao, M.; Wu, Z.; Zhang, D.; Zhang, C.; Xiao, Y.; Chu, M.; Genest, A.; et al. Ru-Catalyzed Reverse Water Gas Shift Reaction with Near-Unity Selectivity and Superior Stability. *ACS Mater. Lett.* **2021**, *3*, 1652–1659. [CrossRef] [PubMed]
87. Tawalbeh, M.; Javed, R.M.N.; Al-Othman, A.; Almomani, F.; Ajith, S. Unlocking the potential of CO_2 hydrogenation into valuable products using noble metal catalysts: A comprehensive review. *Environ. Technol. Innov.* **2023**, *31*, 103217. [CrossRef]
88. Pakhare, D.; Spivey, J. A review of dry (CO_2) reforming of methane over noble metal catalysts. *Chem. Soc. Rev.* **2014**, *43*, 7813–7837. [CrossRef]
89. Ojelade, O.A.; Zaman, S.F. A Review on Pd Based Catalysts for CO_2 Hydrogenation to Methanol: In-Depth Activity and DRIFTS Mechanistic Study. *Catal. Surv. Asia* **2020**, *24*, 11–37. [CrossRef]
90. Kattel, S.; Liu, P.; Chen, J.G.G. Tuning Selectivity of CO_2 Hydrogenation Reactions at the Metal/Oxide Interface. *J. Am. Chem. Soc.* **2017**, *139*, 9739–9754. [CrossRef]
91. Al-Mamoori, A.; Rownaghi, A.A.; Rezaei, F. Combined capture and utilization of CO_2 for syngas production over dual-function materials. *ACS Sustain. Chem. Eng.* **2018**, *6*, 13551–13561. [CrossRef]
92. Arellano-Treviño, M.A.; He, Z.; Libby, M.C.; Farrauto, R.J. Catalysts and adsorbents for CO_2 capture and conversion with dual function materials: Limitations of Ni-containing DFMs for flue gas applications. *J. CO_2 Util.* **2019**, *31*, 143–151. [CrossRef]
93. Duyar, M.S.; Wang, S.; Arellano-Treviño, M.A.; Farrauto, R.J. CO_2 utilization with a novel dual function material (DFM) for capture and catalytic conversion to synthetic natural gas: An update. *J. CO_2 Util.* **2016**, *15*, 65–71. [CrossRef]
94. Proaño, L.; Arellano-Treviño, M.A.; Farrauto, R.J.; Figueredo, M.; Jeong-Potter, C.; Cobo, M. Mechanistic assessment of dual function materials, composed of Ru-Ni, Na_2O/Al_2O_3 and Pt-Ni, Na_2O/Al_2O_3, for CO_2 capture and methanation by in-situ DRIFTS. *Appl. Surf. Sci.* **2020**, *533*, 147469. [CrossRef]
95. Proaño, L.; Tello, E.; Arellano-Trevino, M.A.; Wang, S.; Farrauto, R.J.; Cobo, M. In-situ DRIFTS study of two-step CO_2 capture and catalytic methanation over Ru,"Na_2O"/Al_2O_3 Dual Functional Material. *Appl. Surf. Sci.* **2019**, *479*, 25–30. [CrossRef]
96. Bermejo-López, A.; Pereda-Ayo, B.; González-Marcos, J.A.; González-Velasco, J.R. Mechanism of the CO_2 storage and in situ hydrogenation to CH4. Temperature and adsorbent loading effects over Ru-CaO/Al_2O_3 and Ru-Na_2CO_3/Al_2O_3 catalysts. *Appl. Catal. B Environ.* **2019**, *256*, 117845. [CrossRef]
97. Bobadilla, L.F.; Riesco-García, J.M.; Penelás-Pérez, G.; Urakawa, A. Enabling continuous capture and catalytic conversion of flue gas CO_2 to syngas in one process. *J. CO_2 Util.* **2016**, *14*, 106–111. [CrossRef]
98. Wang, S.; Farrauto, R.J.; Karp, S.; Jeon, J.H.; Schrunk, E.T. Parametric, cyclic aging and characterization studies for CO_2 capture from flue gas and catalytic conversion to synthetic natural gas using a dual functional material (DFM). *J. CO_2 Util.* **2018**, *27*, 390–397. [CrossRef]
99. Hu, L.; Urakawa, A. Continuous CO_2 capture and reduction in one process: CO_2 methanation over unpromoted and promoted Ni/ZrO2. *J. CO_2 Util.* **2018**, *25*, 323–329. [CrossRef]
100. Arellano-Treviño, M.A.; Kanani, N.; Jeong-Potter, C.W.; Farrauto, R.J. Bimetallic catalysts for CO_2 capture and hydrogenation at simulated flue gas conditions. *Chem. Eng. J.* **2019**, *375*, 121953. [CrossRef]
101. Bermejo-López, A.; Pereda-Ayo, B.; González-Marcos, J.A.; González-Velasco, J.R. Ni loading effects on dual function materials for capture and in-situ conversion of CO_2 to CH_4 using CaO or Na_2CO_3. *J. CO_2 Util.* **2019**, *34*, 576–587. [CrossRef]
102. Sietsma, J.R.A.; Jos van Dillen, A.; de Jongh, P.E.; de Jong, K.P. Application of ordered mesoporous materials as model supports to study catalyst preparation by impregnation and drying. In *Studies in Surface Science and Catalysis*; Gaigneaux, E.M., Devillers, M., De Vos, D.E., Hermans, S., Jacobs, P.A., Martens, J.A., Ruiz, P., Eds.; Elsevier: Amsterdam, The Netherlands, 2006; Volume 162, pp. 95–102.
103. Lu, Z.; Kunisch, J.; Gan, Z.; Bunian, M.; Wu, T.; Lei, Y. Gold catalysts synthesized using a modified incipient wetness impregnation method for propylene epoxidation. *ChemCatChem* **2020**, *12*, 5993–5999. [CrossRef]
104. Danks, A.E.; Hall, S.R.; Schnepp, Z. The evolution of 'sol–gel' chemistry as a technique for materials synthesis. *Mater. Horiz.* **2016**, *3*, 91–112. [CrossRef]
105. Wu, J.; Zheng, Y.; Fu, J.; Guo, Y.; Yu, J.; Chu, J.; Huang, P.; Zhao, C. Synthetic Ni–CaO–CeO_2 dual function materials for integrated CO_2 capture and conversion via reverse water–gas shift reaction. *Sep. Purif. Technol.* **2023**, *317*, 123916. [CrossRef]
106. Pechini, M.P. Method of Preparing Lead and Alkaline Earth Titanates and Niobates and Coating Method Using the Same to Form a Capacitor. U.S. Patent US304434A, 11 July 1967.

107. Sunde, T.O.L.; Grande, T.; Einarsrud, M.-A. Modified pechini synthesis of oxide powders and thin films. In *Handbook of Sol-Gel Science and Technology*; Springer: Berlin/Heidelberg, Germany, 2016.
108. Radfarnia, H.R.; Sayari, A. A highly efficient CaO-based CO_2 sorbent prepared by a citrate-assisted sol–gel technique. *Chem. Eng. J.* **2015**, *262*, 913–920. [CrossRef]
109. Jin, S.; Bang, G.; Liu, L.; Lee, C.-H. Synthesis of mesoporous MgO–CeO_2 composites with enhanced CO_2 capture rate via controlled combustion. *Microporous Mesoporous Mater.* **2019**, *288*, 109587. [CrossRef]
110. Ma, X.; Li, X.; Cui, H.; Zhang, W.; Cheng, Z.; Zhou, Z. Metal oxide-doped Ni/CaO dual-function materials for integrated CO_2 capture and conversion: Performance and mechanism. *AIChE J.* **2023**, *69*, e17520. [CrossRef]
111. Sun, H.; Wang, J.; Zhao, J.; Shen, B.; Shi, J.; Huang, J.; Wu, C. Dual functional catalytic materials of Ni over Ce-modified CaO sorbents for integrated CO_2 capture and conversion. *Appl. Catal. B Environ.* **2019**, *244*, 63–75. [CrossRef]
112. Zhang, X.; Liu, W.; Peng, P.; Zhang, Z.; Du, Q.; Shi, J.; Deng, L. A dual functional sorbent/catalyst material for in-situ CO_2 capture and conversion to ethylene production. *Fuel* **2023**, *351*, 128701. [CrossRef]
113. Machida, M.; Uto, M.; Kijima, T. Preparation of large surface area MnOx-ZrO_2 for sorptive NOx removal. In *Studies in Surface Science and Catalysis*; Elsevier: Amsterdam, The Netherlands, 2000; Volume 143, pp. 855–862.
114. Virji, M.; Stefaniak, A. *A Review of Engineered Nanomaterial Manufacturing Processes and Associated Exposures*; Elsevier: Amsterdam, The Netherlands, 2014.
115. Li, C.; Li, M.; van Veen, A.C. Synthesis of Nano-Catalysts in Flow Conditions Using Millimixers. In *Advanced Nanomaterials for Catalysis and Energy*; Elsevier: Amsterdam, The Netherlands, 2019; pp. 1–28.
116. Molina-Ramírez, S.; Cortés-Reyes, M.; Herrera, C.; Larrubia, M.; Alemany, L. CO_2-SR Cyclic Technology: CO_2 Storage and in situ Regeneration with CH4 over a new dual function NiBa unsupported catalyst. *J. CO_2 Util.* **2020**, *40*, 101201. [CrossRef]
117. Karami, D.; Mahinpey, N. Study of Al_2O_3 addition to synthetic Ca-based sorbents for CO_2 sorption capacity and stability in cyclic operations. *Can. J. Chem. Eng.* **2015**, *93*, 102–110. [CrossRef]
118. Huang, P.; Chu, J.; Fu, J.; Yu, J.; Li, S.; Guo, Y.; Zhao, C.; Liu, J. Influence of reduction conditions on the structure-activity relationships of $NaNO_3$-promoted Ni/MgO dual function materials for integrated CO_2 capture and methanation. *Chem. Eng. J.* **2023**, *467*, 143431. [CrossRef]
119. Wegener Kofoed, M.V.; Jensen, M.B.; Mørck Ottosen, L.D. Chapter 12—Biological upgrading of biogas through CO_2 conversion to CH4. In *Emerging Technologies and Biological Systems for Biogas Upgrading*; Aryal, N., Mørck Ottosen, L.D., Wegener Kofoed, M.V., Pant, D., Eds.; Academic Press: Cambridge, MA, USA, 2021; pp. 321–362. [CrossRef]
120. Seemann, M.; Thunman, H. 9—Methane synthesis. In *Substitute Natural Gas from Waste*; Materazzi, M., Foscolo, P.U., Eds.; Academic Press: Cambridge, MA, USA, 2019; pp. 221–243. [CrossRef]
121. Sun, H.; Zhang, Y.; Guan, S.; Huang, J.; Wu, C. Direct and highly selective conversion of captured CO_2 into methane through integrated carbon capture and utilization over dual functional materials. *J. CO_2 Util.* **2020**, *38*, 262–272. [CrossRef]
122. Kosaka, F.; Liu, Y.; Chen, S.-Y.; Mochizuki, T.; Takagi, H.; Urakawa, A.; Kuramoto, K. Enhanced Activity of Integrated CO_2 Capture and Reduction to CH4 under Pressurized Conditions toward Atmospheric CO_2 Utilization. *ACS Sustain. Chem. Eng.* **2021**, *9*, 3452–3463. [CrossRef]
123. Porta, A.; Matarrese, R.; Visconti, C.G.; Castoldi, L.; Lietti, L. Storage Material Effects on the Performance of Ru-Based CO_2 Capture and Methanation Dual Functioning Materials. *Ind. Eng. Chem. Res.* **2021**, *60*, 6706–6718. [CrossRef]
124. Jeong-Potter, C.; Farrauto, R. Feasibility Study of Combining Direct Air Capture of CO_2 and Methanation at Isothermal Conditions with Dual Function Materials. *Appl. Catal. B Environ.* **2021**, *282*, 119416. [CrossRef]
125. Sun, H.; Wang, Y.; Xu, S.; Osman, A.I.; Stenning, G.; Han, J.; Sun, S.; Rooney, D.; Williams, P.T.; Wang, F.; et al. Understanding the interaction between active sites and sorbents during the integrated carbon capture and utilization process. *Fuel* **2021**, *286*, 119308. [CrossRef]
126. Porta, A.; Visconti, C.G.; Castoldi, L.; Matarrese, R.; Jeong-Potter, C.; Farrauto, R.; Lietti, L. Ru-Ba synergistic effect in dual functioning materials for cyclic CO_2 capture and methanation. *Appl. Catal. B Environ.* **2021**, *283*, 119654. [CrossRef]
127. Cimino, S.; Russo, R.; Lisi, L. Insights into the cyclic CO_2 capture and catalytic methanation over highly performing Li-Ru/Al_2O_3 dual function materials. *Chem. Eng. J.* **2022**, *428*, 131275. [CrossRef]
128. Onrubia-Calvo, J.A.; Bermejo-López, A.; Pérez-Vázquez, S.; Pereda-Ayo, B.; González-Marcos, J.A.; González-Velasco, J.R. Applicability of $LaNiO_3$-derived catalysts as dual function materials for CO_2 capture and in-situ conversion to methane. *Fuel* **2022**, *320*, 123842. [CrossRef]
129. Sun, Z.; Shao, B.; Zhang, Y.; Gao, Z.; Wang, M.; Liu, H.; Hu, J. Integrated CO_2 capture and methanation from the intermediate-temperature flue gas on dual functional hybrids of AMS/CaMgO||NixCoy. *Sep. Purif. Technol.* **2023**, *307*, 122680. [CrossRef]
130. Faria, A.C.; Trujillano, R.; Rives, V.; Miguel, C.V.; Rodrigues, A.E.; Madeira, L.M. Cyclic operation of CO_2 capture and conversion into methane on Ni-hydrotalcite based dual function materials (DFMs). *J. CO_2 Util.* **2023**, *72*, 102476. [CrossRef]
131. Onrubia-Calvo, J.A.; Bermejo-López, A.; Pereda-Ayo, B.; González-Marcos, J.A.; González-Velasco, J.R. Ca doping effect on the performance of La1−xCaxNiO_3/CeO_2-derived dual function materials for CO_2 capture and hydrogenation to methane. *Appl. Catal. B Environ.* **2023**, *321*, 122045. [CrossRef]
132. Sakai, M.; Imagawa, H.; Baba, N. Layered-double-hydroxide-based Ni catalyst for CO_2 capture and methanation. *Appl. Catal. A Gen.* **2022**, *647*, 118904. [CrossRef]

133. Catarina Faria, A.; Miguel, C.V.; Ferreira, A.F.P.; Rodrigues, A.E.; Madeira, L.M. CO_2 capture and conversion to methane with Ni-substituted hydrotalcite dual function extrudates. *Chem. Eng. J.* **2023**, *476*, 146539. [CrossRef]
134. Wang, X.; Economides, M. CHAPTER 7—Gas-To-Liquids (GTL). In *Advanced Natural Gas Engineering*; Wang, X., Economides, M., Eds.; Gulf Publishing Company: Houston, TX, USA, 2009; pp. 243–287. [CrossRef]
135. Cimino, S.; Boccia, F.; Lisi, L. Effect of alkali promoters (Li, Na, K) on the performance of Ru/Al_2O_3 catalysts for CO_2 capture and hydrogenation to methane. *J. CO_2 Util.* **2020**, *37*, 195–203. [CrossRef]
136. Jeong-Potter, C.; Zangiabadi, A.; Farrauto, R. Extended aging of Ru-Ni, Na_2O/Al_2O_3 dual function materials (DFM) for combined capture and subsequent catalytic methanation of CO_2 from power plant flue gas. *Fuel* **2022**, *328*, 125283. [CrossRef]
137. Bermejo-López, A.; Pereda-Ayo, B.; González-Marcos, J.A.; González-Velasco, J.R. Simulation-based optimization of cycle timing for CO_2 capture and hydrogenation with dual function catalyst. *Catal. Today* **2022**, *394–396*, 314–324. [CrossRef]
138. Bermejo-López, A.; Pereda-Ayo, B.; González-Marcos, J.A.; González-Velasco, J.R. Modeling the CO_2 capture and in situ conversion to CH4 on dual function Ru-Na_2CO_3/Al_2O_3 catalyst. *J. CO_2 Util.* **2020**, *42*, 101351. [CrossRef]
139. Garbarino, G.; Bellotti, D.; Finocchio, E.; Magistri, L.; Busca, G. Methanation of carbon dioxide on Ru/Al_2O_3: Catalytic activity and infrared study. *Catal. Today* **2016**, *277*, 21–28. [CrossRef]
140. Dreyer, J.A.H.; Li, P.; Zhang, L.; Beh, G.K.; Zhang, R.; Sit, P.H.L.; Teoh, W.Y. Influence of the oxide support reducibility on the CO_2 methanation over Ru-based catalysts. *Appl. Catal. B Environ.* **2017**, *219*, 715–726. [CrossRef]
141. González-Castaño, M.; Dorneanu, B.; Arellano-García, H. The reverse water gas shift reaction: A process systems engineering perspective. *React. Chem. Eng.* **2021**, *6*, 954–976. [CrossRef]
142. Shao, B.; Hu, G.; Alkebsi, K.A.M.; Ye, G.; Lin, X.; Du, W.; Hu, J.; Wang, M.; Liu, H.; Qian, F. Heterojunction-redox catalysts of FexCoyMg10CaO for high-temperature CO_2 capture and in situ conversion in the context of green manufacturing. *Energy Environ. Sci.* **2021**, *14*, 2291–2301. [CrossRef]
143. Sun, S.; He, S.; Wu, C. Ni promoted Fe-CaO dual functional materials for calcium chemical dual looping. *Chem. Eng. J.* **2022**, *441*, 135752. [CrossRef]
144. Sasayama, T.; Kosaka, F.; Liu, Y.Y.; Yamaguchi, T.; Chen, S.Y.; Mochizuki, T.; Urakawa, A.; Kuramoto, K. Integrated CO_2 capture and selective conversion to syngas using transition-metal-free Na/Al_2O_3 dual-function material. *J. CO_2 Util.* **2022**, *60*, 102049. [CrossRef]
145. Li, L.; Miyazaki, S.; Yasumura, S.; Ting, K.W.; Toyao, T.; Maeno, Z.; Shimizu, K.-I. Continuous CO_2 Capture and Selective Hydrogenation to CO over Na-Promoted Pt Nanoparticles on Al_2O_3. *ACS Catal.* **2022**, *12*, 2639–2650. [CrossRef]
146. Guo, Y.; Wang, G.; Yu, J.; Huang, P.; Sun, J.; Wang, R.; Wang, T.; Zhao, C. Tailoring the performance of Ni-CaO dual function materials for integrated CO_2 capture and conversion by doping transition metal oxides. *Sep. Purif. Technol.* **2023**, *305*, 122455. [CrossRef]
147. Sun, S.; Zhang, C.; Guan, S.; Xu, S.; Williams, P.T.; Wu, C. Ni/support-CaO bifunctional combined materials for integrated CO_2 capture and reverse water-gas shift reaction: Influence of different supports. *Sep. Purif. Technol.* **2022**, *298*, 121604. [CrossRef]
148. Bao, Z.; Yu, F. Chapter Two—Catalytic Conversion of Biogas to Syngas via Dry Reforming Process. In *Advances in Bioenergy*; Li, Y., Ge, X., Eds.; Elsevier: Amsterdam, The Netherlands, 2018; Volume 3, pp. 43–76.
149. Hu, J.; Hongmanorom, P.; Galvita, V.V.; Li, Z.; Kawi, S. Bifunctional Ni-Ca based material for integrated CO_2 capture and conversion via calcium-looping dry reforming. *Appl. Catal. B Environ.* **2021**, *284*, 119734. [CrossRef]
150. Kim, S.M.; Abdala, P.M.; Broda, M.; Hosseini, D.; Copéret, C.; Müller, C. Integrated CO_2 Capture and Conversion as an Efficient Process for Fuels from Greenhouse Gases. *ACS Catal.* **2018**, *8*, 2815–2823. [CrossRef]
151. Zhao, Y.; Li, Y.; Jin, B.; Liang, Z. Layered double hydroxide derived bifunctional Ca-Fe-Mg material for integrated CO_2 capture and utilization via chemical looping strategy. *Chem. Eng. J.* **2022**, *431*, 133826. [CrossRef]
152. Tian, S.; Yan, F.; Zhang, Z.; Jiang, J. Calcium-looping reforming of methane realizes in situ CO_2 utilization with improved energy efficiency. *Sci. Adv.* **2019**, *5*, eaav5077. [CrossRef]
153. Jo, S.B.; Woo, J.H.; Lee, J.H.; Kim, T.Y.; Kang, H.I.; Lee, S.C.; Kim, J.C. CO_2 green technologies in CO_2 capture and direct utilization processes: Methanation, reverse water-gas shift, and dry reforming of methane. *Sustain. Energy Fuels* **2020**, *4*, 5543–5549. [CrossRef]
154. Hu, J.; Hongmanorom, P.; Chirawatkul, P.; Kawi, S. Efficient integration of CO_2 capture and conversion over a Ni supported CeO_2-modified CaO microsphere at moderate temperature. *Chem. Eng. J.* **2021**, *426*, 130864. [CrossRef]
155. Merkouri, L.-P.; Ramirez Reina, T.; Duyar, M.S. Feasibility of switchable dual function materials as a flexible technology for CO_2 capture and utilisation and evidence of passive direct air capture. *Nanoscale* **2022**, *14*, 12620–12637. [CrossRef] [PubMed]
156. Law, Z.X.; Pan, Y.-T.; Tsai, D.-H. Calcium looping of CO_2 capture coupled to syngas production using Ni-CaO-based dual functional material. *Fuel* **2022**, *328*, 125202. [CrossRef]
157. Hussain, I.; Tanimu, G.; Ahmed, S.; Aniz, C.U.; Alasiri, H.; Alhooshani, K. A review of the indispensable role of oxygen vacancies for enhanced CO_2 methanation activity over CeO_2-based catalysts: Uncovering, influencing, and tuning strategies. *Int. J. Hydrogen Energy* **2023**, *48*, 24663–24696. [CrossRef]